Transactions in Theoretical and Mathematical Physics

Publisher: Qom University of Technology

ISSN: 3041-8984

Volume**:** 3, Issue 1, 2026

Available online: https://ttmp.qut.ac.ir

Table of Contents

TTMP vol 3 (1), 2026
doi: 10.30511/TTMP.2026.2081057.1069

Transactions in Theoretical and Mathematical Physics

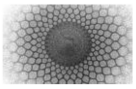

Analysis of the Viscous Laminar Flow in a Straight Pipe Based on the Complex Variable Finite Difference Method

Song-Chol Ri[1][a], **InGu Jo**[1], **Namsu Pak**[1]

[1] Faculty of Aerospace Engineering, Kim Chaek University of Technology, Pyongyang, Democratic People's Republic of Korea

Received: 16 December 2025 / Accepted: 21 February 2026 / Published: 22 February 2026

Abstract

The paper describes an efficient complex variable finite difference method (CVFDM) for calculating the two-dimensional potential flow, the viscous laminar flow in the straight pipe. The theoretical development is based on the generalization of the Cauchy-Riemann differential equation into the finite difference equation in terms of a complex variable to solve a two-dimensional boundary value problem. A numerical code is developed by this method and analytical solutions are obtained for illustrative problems. The validation of this method is confirmed through the analytical solutions for Pois-euille flow and Couette flow.

Keywords: Complex variable finite difference method; Cauchy-Riemann equation; Poiseuille flow; Couette flow

1 Introduction

The mathematical approach to an approximate method for solving the two-dimensional boundary value problems has been studied by many researchers, of which the complex variable boundary element method (CVBEM) and the complex variable finite element method (ZFEM) are typical methods.

Hromadka and Lai [1] derived a complex variable boundary element method (CVBEM) for solving numerically the problems governed by the two-dimensional Laplace equation. The potential flow past single and multicomponent airfoils in free air, in ground effect, in an infinite cascade, and in perforated wall wind tunnels, is calculated by the complex variable boundary element method algorithm [2]. Dumir *et al.* [3] presented a complex variable boundary element method for torsion of anisotropic cylindrical/prismatic bars whose longitudinal axis is normal to the plane of elastic symmetry of the bar. Satao [4] calculated the potential flow in the presence of thin objects based on the complex variable boundary element method. An accurate complex variable boundary element method is proposed for solving the two-dimensional boundary value problems governed by a steady-state advection-diffusion-reaction equation [5].

Tamayo *et al.* [6] applied a virtual crack extension technique using the complex variable finite element method (ZFEM) to the thermoplastic fracture problems. This virtual crack extension approach provided an accurate computation of the energy release rate as a byproduct of the complex variable finite element analysis without using energy conservation integrals. Millwater *et al.* [7] proposed the virtual crack extension method based on the complex variable finite element method and computed the energy release rate as a numerical derivative of the strain energy with respect to a crack extension using the complex Taylor series expansion method. Fielder *et al.* [8] detailed the application of the complex variable finite element method, ZFEM, to structures containing residual stresses. A thick-walled sphere model in which the residual stress field is induced by an autofrettage process, is considered. Since the results of ZFEM partial derivative results show high accuracy compared with standard finite element solutions, ZFEM is an effective step-size independent method for calculating shape, material, and loading sensitivities of structures subjected to residual stresses.

Restrepo *et al.* [9] combined the finite element method with the complex variable differentiation theory to calculate the first-order sensitivities for transient heat transfer equations accurately and reduced the computational time compared to traditional sensitivity analysis methods. Millwater *et al.* [10] computed accurate sensitivities with respect to the unknown parameters by solving an inverse finite element optimization problem using the complex variable finite

[a]Corresponding author: rsc83320@star-co.net.kp

element method, ZFEM, and proposed the use of full-field kinematic measurements to determine the constitutive material properties. Aaron Rios *et al.* [11] developed a complex variable transient thermo-mechanical element and used it to calculate accurate sensitivities of the thermal and stress time-dependent responses of a thick wall cylinder with temperature-dependent material properties using the complex Taylor series expansion (CTSE).

In this paper, the complex variable finite difference method (CVFDM) is introduced to analyze the two-dimensional potential problem. To calculate the velocity distribution of viscous laminar flow in a straight pipe, the Cauchy-Riemann differential equation is generalized to a complex finite difference equation and solve as a two-dimensional boundary value problem. The numerical results of CVFDM for the laminar flow velocity of a steady viscous fluid in a straight pipe are compared with the available analytical solutions to verify the proposed method.

2 The theoretical background of a complex variable finite difference method

The complex variable finite difference method is based on the Cauchy-Riemann equations. We will consider the complex variable function $F(z) = \psi + i\phi$ continued on boundary Γ of domain Ω (see Fig. 1), in which real part ψ and imaginary part ϕ satisfy the Cauchy-Riemann equations and Laplace's equation respectively.

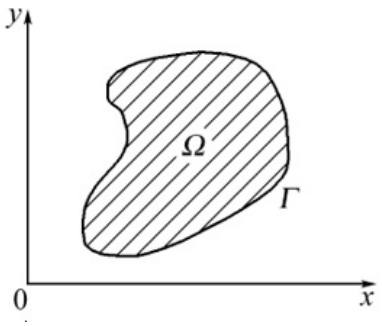

Fig. 1 Domain Ω enclosed by boundary curve Γ.

$$\begin{aligned}\frac{\partial\psi}{\partial x} &= \frac{\partial\phi}{\partial y},\\ \frac{\partial\psi}{\partial y} &= -\frac{\partial\phi}{\partial x}.\end{aligned} \tag{1}$$

Now we convert the Cauchy-Riemann equations into difference equations (see Fig. 2). The values of analytic function $F(z) = \psi + i\phi$ on the points A, B, C, D and O are described as $F_{i,j+1}$, $F_{i-1,j}$, $F_{i,j-1}$, $F_{i+1,j}$ and $F_{i,j}$.

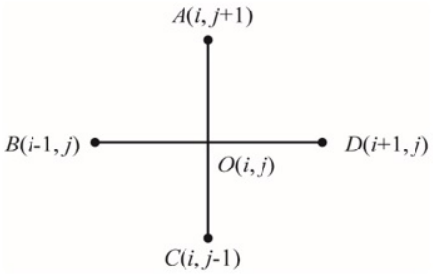

Fig. 2 Difference scheme.

By converting Eq. (1) into forward difference scheme,

$$\begin{aligned}\frac{\psi_{i+1,j}-\psi_{i,j}}{\Delta x} &= \frac{\phi_{i,j+1}-\phi_{i,j}}{\Delta y},\\ \frac{\psi_{i,j+1}-\psi_{i,j}}{\Delta y} &= -\frac{\phi_{i+1,j}-\phi_{i,j}}{\Delta x}.\end{aligned} \tag{2}$$

We introduce $\Delta y/\Delta x = k$ in the above equation. Then we deform the above equations, respectively,

$$\begin{aligned}\psi_{i+1,j}-\psi_{i,j} &= \frac{1}{k}(\phi_{i,j+1}-\phi_{i,j}),\\ \psi_{i,j+1}-\psi_{i,j} &= -k(\phi_{i+1,j}-\phi_{i,j}).\end{aligned} \tag{3}$$

We introduce the mathematical symbols *Re* (real part) and *Im* (imaginary part) on Eq. (3). Then

$$\begin{aligned}Re(F_{i+1,j}-F_{i,j}) &= \frac{1}{k}Im(F_{i,j+1}-F_{i,j}),\\ Re(F_{i,j+1}-F_{i,j}) &= -kIm(F_{i+1,j}-F_{i,j}).\end{aligned} \tag{4}$$

By accounting Eq. (4),

$$\begin{aligned}F_{i+1,j}-F_{i,j} =& Re(F_{i+1,j}-F_{i,j})+iIm(F_{i+1,j}-F_{i,j})\\ =& \frac{1}{k}Im(F_{i,j+1}-F_{i,j})-\frac{i}{k}Re(F_{i,j+1}-F_{i,j})\\ =& -\frac{i}{k}Re(F_{i,j+1}-F_{i,j})+\frac{1}{k}Im(F_{i,j+1}-F_{i,j})\\ =& -\frac{i}{k}\left[Re(F_{i,j+1}-F_{i,j})+iIm(F_{i,j+1}-F_{i,j})\right]\\ =& -\frac{i}{k}\left[(ReF_{i,j+1}+iImF_{i,j+1})-(ReF_{i,j}+iImF_{i,j})\right]\\ =& -\frac{i}{k}(F_{i,j+1}-F_{i,j}).\end{aligned} \tag{5}$$

By deforming the above equation,

$$F_{i+1,j}-F_{i,j} = -\frac{i}{k}(F_{i,j+1}-F_{i,j}), \tag{6}$$

or

$$kF_{i+1,j}-(k+i)F_{i,j}+iF_{i,j+1} = 0. \tag{7}$$

By deforming the difference scheme of Eq. (1) into backward difference scheme,

$$\frac{\psi_{i,j}-\psi_{i-1,j}}{\Delta x}=\frac{\phi_{i,j}-\phi_{i,j-1}}{\Delta y},$$
$$\frac{\psi_{i,j}-\psi_{i,j-1}}{\Delta y}=-\frac{\phi_{i,j}-\phi_{i-1,j}}{\Delta x}. \quad (8)$$

By arranging the above equation similarly,

$$kF_{i-1,j}-(k+i)F_{i,j}+iF_{i,j-1}=0. \quad (9)$$

By applying central difference to Eq. (1),

$$\frac{\psi_{i+1,j}-\psi_{i-1,j}}{2\Delta x}=\frac{\phi_{i,j+1}-\phi_{i,j-1}}{2\Delta y},$$
$$\frac{\psi_{i,j+1}-\psi_{i,j-1}}{2\Delta y}=-\frac{\phi_{i+1,j}-\phi_{i-1,j}}{2\Delta x}. \quad (10)$$

By arranging the above equation,

$$k(F_{i+1,j}-F_{i-1,j})+i(F_{i,j+1}-F_{i,j-1})=0. \quad (11)$$

We will consider one method of solving Eqs. (7), (9) and (11). We divide rectangular element EFGH by using a horizontal line BD and a vertical AC, make 4 elementary rectangles such as EBOA, AODH, BFCO and OCGD (see Fig. 3).

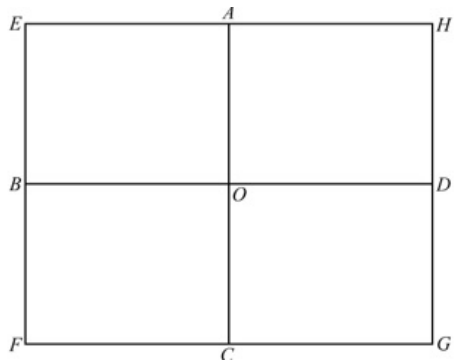

Fig. 3 Dividing of rectangular element.

Here $F_{i,j+1}(A)$, $F_{i-1,j}(B)$, $F_{i,j-1}(C)$, $F_{i+1,j}(D)$, $F_{i-1,j+1}(E)$, $F_{i-1,j-1}(F)$, $F_{i+1,j-1}(G)$, $F_{i+1,j+1}(H)$ and $F_{i,j}(O)$ are values of complex function on the angular points A,B,C,D,E,F,G,H and O,

$$F_A=\psi_{i,j+1}+i\phi_{i,j+1},$$
$$F_B=\psi_{i-1,j}+i\phi_{i-1,j},$$
$$F_C=\psi_{i,j-1}+i\phi_{i,j-1},$$
$$F_D=\psi_{i+1,j}+i\phi_{i+1,j},$$
$$F_E=\psi_{i-1,j+1}+i\phi_{i-1,j+1},$$
$$F_F=\psi_{i-1,j-1}+i\phi_{i-1,j-1},$$
$$F_G=\psi_{i+1,j-1}+i\phi_{i+1,j-1},$$
$$F_H=\psi_{i+1,j+1}+i\phi_{i+1,j+1},$$
$$F_O=\psi_{i,j}+i\phi_{i,j},$$

where $\psi_{i,j+1}$, $\psi_{i-1,j}$, $\psi_{i,j-1}$, $\psi_{i+1,j}$, $\psi_{i-1,j+1}$, $\psi_{i-1,j-1}$, $\psi_{i+1,j-1}$ and $\psi_{i+1,j+1}$ are 8 known, and $\psi_{i,j}$, $\phi_{i,j}$, $\phi_{i,j+1}$, $\phi_{i-1,j}$, $\phi_{i,j-1}$, $\phi_{i+1,j}$, $\phi_{i-1,j+1}$, $\phi_{i-1,j-1}$, $\phi_{i+1,j-1}$ and $\phi_{i+1,j+1}$ are 10 unknowns. We make the matrix form as follows to solve the 1^{st} polynomial systems of equations with 10 unknowns.

$$\begin{pmatrix} -k & 0 & 0 & 0 & -1 & 1 & 0 & 0 & 0 & 0\\ -1 & 0 & k & 0 & 0 & -k & 0 & 0 & 0 & 0\\ -k & 0 & 0 & 0 & 0 & 1 & -1 & 0 & 0 & 0\\ -1 & 0 & 0 & 0 & 0 & -k & 0 & 0 & k & 0\\ 0 & 0 & 0 & 0 & 0 & 0 & 0 & 0 & -1 & 1\\ 0 & 0 & 0 & 0 & 0 & 0 & k & 0 & 0 & -k\\ 0 & 1 & -1 & 0 & 0 & 0 & 0 & 0 & 0 & 0\\ 0 & -k & 0 & 0 & k & 0 & 0 & 0 & 0 & 0\\ 0 & 1 & 0 & -1 & 0 & 0 & 0 & 0 & 0 & 0\\ 0 & -k & 0 & 0 & 0 & 0 & 0 & k & 0 & 0 \end{pmatrix}$$
$$\times\begin{pmatrix} \psi_{ij}\\ \phi_{i-1,j-1}\\ \phi_{i-1,j}\\ \phi_{i-1,j+1}\\ \phi_{i,j-1}\\ \phi_{i,j}\\ \phi_{i,j+1}\\ \phi_{i+1,j-1}\\ \phi_{i+1,j}\\ \phi_{i+1,j+1} \end{pmatrix}=\begin{pmatrix} -k\psi_{i-1,j}\\ -\psi_{i,j-1}\\ -k\psi_{i+1,j}\\ -\psi_{i,j+1}\\ -k\psi_{i,j+1}+k\psi_{i+1,j+1}\\ \psi_{i+1,j+1}-\psi_{i+1,j}\\ -k\psi_{i,j-1}+k\psi_{i-1,j-1}\\ \psi_{i-1,j-1}-\psi_{i-1,j}\\ -k\psi_{i+1,j-1}+k\psi_{i-1,j-1}\\ \psi_{i-1,j-1}-\psi_{i-1,j+1} \end{pmatrix}. \quad (12)$$

We can calculate the unknowns ψ and ϕ in the domain and on the boundary by solving these matrix equations. We will compare an error between Cauchy-Riemann differential equation and Laplace differential equation. The difference form of Laplace equation can be expressed as

$$\frac{\psi_{i+1,j}-2\psi_{i,j}+\psi_{i-1,j}}{h^2}+\frac{\psi_{i,j+1}-2\psi_{i,j}+\psi_{i,j-1}}{k^2}=\overline{L_1(\psi)} \quad (13)$$

where h is a x-direction length of elementary rectangle, k is y-direction length of elementary rectangle. By introducing equation $k=\delta h$

$$\overline{L_1(\psi)}=\frac{1}{h^2}\Big[(\psi_{i+1,j}-2\psi_{i,j}+\psi_{i-1,j})+\frac{1}{\delta^2}(\psi_{i,j+1}-2\psi_{i,j}+\psi_{i,j-1})\Big]. \quad (14)$$

By expressing the error between Eq. (14) and Laplace equation as $R_1(\psi)$,

$$R_1(\psi)=\overline{L_1(\psi)}-L_1(\psi),$$

where $L_1(\psi)$ is an error of Laplace differential equation. Therefore,

$$L_1(\psi)=\frac{\partial^2\psi}{\partial x^2}+\frac{\partial^2\psi}{\partial y^2},$$

Because $L_1(\psi)=0$,

$$\begin{aligned}R_1(\psi)=&\frac{1}{h^2}\Big[\Big(\psi_{i,j}+h\frac{\partial\psi_{i,j}}{\partial x}+\frac{h^2}{2!}\frac{\partial^2\psi_{i,j}}{\partial x^2}+\frac{h^3}{3!}\frac{\partial^3\psi_{i,j}}{\partial x^3}\\&+\frac{h^4}{4!}\frac{\partial^4\psi_{i,j}}{\partial x^4}+\frac{h^5}{5!}\frac{\partial^5\psi_{i,j}}{\partial x^5}+\frac{h^6}{6!}\frac{\partial^6\psi_{i,j}}{\partial x^6}-2\psi_{i,j}\\&+\psi_{i,j}-h\frac{\partial\psi_{i,j}}{\partial x}+\frac{h^2}{2!}\frac{\partial^2\psi_{i,j}}{\partial x^2}-\frac{h^3}{3!}\frac{\partial^3\psi_{i,j}}{\partial x^3}\\&+\frac{h^4}{4!}\frac{\partial^4\psi_{i,j}}{\partial x^4}-\frac{h^5}{5!}\frac{\partial^5\psi_{i,j}}{\partial x^5}+\frac{h^6}{6!}\frac{\partial^6\psi_{i,j}}{\partial x^6}\Big)\\&+\frac{1}{\delta^2}\Big(\psi_{i,j}+k\frac{\partial\psi_{i,j}}{\partial y}+\frac{k^2}{2!}\frac{\partial^2\psi_{i,j}}{\partial y^2}+\frac{k^3}{3!}\frac{\partial^3\psi_{i,j}}{\partial y^3}\\&+\frac{k^4}{4!}\frac{\partial^4\psi_{i,j}}{\partial y^4}+\frac{k^5}{5!}\frac{\partial^5\psi_{i,j}}{\partial y^5}+\frac{k^6}{6!}\frac{\partial^6\psi_{i,j}}{\partial y^6}-2\psi_{i,j}\\&+\psi_{i,j}-k\frac{\partial\psi_{i,j}}{\partial y}+\frac{k^2}{2!}\frac{\partial^2\psi_{i,j}}{\partial y^2}-\frac{k^3}{3!}\frac{\partial^3\psi_{i,j}}{\partial y^3}\\&+\frac{k^4}{4!}\frac{\partial^4\psi_{i,j}}{\partial y^4}-\frac{k^5}{5!}\frac{\partial^5\psi_{i,j}}{\partial y^5}+\frac{k^6}{6!}\frac{\partial^6\psi_{i,j}}{\partial y^6}\Big)\Big]\\&+\mathscr{O}(h^6).\end{aligned}$$

Then,

$$\begin{aligned}R_1(\psi)=&\frac{1}{h^2}\Big[\Big(\frac{\partial^2\psi_{i,j}}{\partial x^2}+\frac{\partial^2\psi_{i,j}}{\partial y^2}\Big)\frac{h^2}{2}\\&+\Big(\frac{\partial^4\psi_{i,j}}{\partial x^4}+\delta^2\frac{\partial^4\psi_{i,j}}{\partial y^4}\Big)\frac{h^4}{12}\\&+\Big(\frac{\partial^6\psi_{i,j}}{\partial x^6}+\delta^4\frac{\partial^6\psi_{i,j}}{\partial y^6}\Big)\frac{h^6}{36}\Big]+\mathscr{O}(h^6),\end{aligned}\tag{15}$$

where

$$\frac{\partial^2\psi_{i,j}}{\partial x^2}=-\frac{\partial^2\psi_{i,j}}{\partial y^2},\qquad\frac{\partial^4\psi_{i,j}}{\partial x^4}=\frac{\partial^4\psi_{i,j}}{\partial y^4},$$
$$\frac{\partial^6\psi_{i,j}}{\partial x^6}=-\frac{\partial^6\psi_{i,j}}{\partial y^6}.$$

Thus,

$$\begin{aligned}R_1(\psi)=&\frac{h^2}{12}(1+\delta^2)\frac{\partial^4\psi_{i,j}}{\partial x^4}+\frac{h^4}{36}(1-\delta^4)\frac{\partial^6\psi_{i,j}}{\partial x^6}\\&+\mathscr{O}(h^6).\end{aligned}\tag{16}$$

If we assume $\delta=1$, then one can easily obtain

$$R_1(\psi)=\frac{h^2}{6}\frac{\partial^4\psi_{i,j}}{\partial x^4}+\mathscr{O}(h^6).\tag{17}$$

Therefore, the error of Laplace differential equation is in the h^2 order. Now we consider an error of Cauchy-Riemann differential equation on the rectangular grid. By applying a forward differential scheme on and backward differential scheme on respectively,

$$\begin{aligned}\frac{\psi_{i+1,j}-\psi_{i,j}}{h}&=\frac{\phi_{i,j}-\phi_{i,j-1}}{k},\\\frac{\phi_{i,j}-\phi_{i-1,j}}{h}&=-\frac{\psi_{i,j+1}-\psi_{i,j}}{k}.\end{aligned}\tag{18}$$

From the above equation,

$$\begin{aligned}\overline{L_2(\psi)}=&\frac{1}{h}\Big[(\psi_{i+1,j}-2\psi_{i,j}+\psi_{i-1,j})\\&+\frac{1}{\delta^2}(\psi_{i,j+1}-2\psi_{i,j}+\psi_{i,j-1})\Big].\end{aligned}\tag{19}$$

By expressing an error of Cauchy-Riemann differential equation as $R_2(\psi)$,

$$R_2(\psi)=\overline{L_2(\psi)}-L_2(\psi),$$

where $L_2(\psi)$ is an error of Cauchy-Riemann differential equation $L_2(\psi)=0$. Thus,

$$\begin{aligned}R_2(\psi)=\overline{L_2(\psi)}=&\frac{1}{h}\Big[(\psi_{i+1,j}-2\psi_{i,j}+\psi_{i-1,j})\\&+\frac{1}{\delta^2}(\psi_{i,j+1}-2\psi_{i,j}+\psi_{i,j-1})\Big].\end{aligned}\tag{20}$$

By using the Tailor series around point (x_i,y_j) of the above equation,

$$\begin{aligned}R_2(\psi)=&\frac{h^3}{12}(1+\delta^2)\frac{\partial^4\psi_{i,j}}{\partial x^4}+\frac{h^5}{36}(1-\delta^4)\frac{\partial^6\psi_{i,j}}{\partial x^6}\\&+\mathscr{O}(h^6).\end{aligned}\tag{21}$$

We can know that the error of Cauchy-Riemann differential equation is the h^3 order from Eq. (21).

Considering a value of $e=R_2(\psi)/R_1(\psi)$, we can know that an error of Cauchy-Riemann differential equation is h times smaller than an error of Laplace differential equation. Generally the error changes with the form of difference scheme. By using the central difference scheme respectively error $R'(\psi)$ is the same as equation (22).

$$\begin{aligned}R'(\psi)=R_2(\psi)=&\frac{8h^3}{12}(1+\delta^2)\frac{\partial^4\psi_{i,j}}{\partial x^4}\\&+\frac{32h^5}{36}(1-\delta^4)\frac{\partial^6\psi_{i,j}}{\partial x^6}+\mathscr{O}(h^6).\end{aligned}\tag{22}$$

From the above equation, we can know that error is 8 times bigger than above error. We will introduce a relaxation method of elevating the convergence of a complex variable difference solution.

$$kF_{i+1,j}-(k+i)F_{i,j}+iF_{i,j+1}=0.\tag{23}$$

By expressing the iterative order as n, the above equation is the same as follows:

$$kF^{n-1}_{i+1,j}-(k+i)F^{n}_{i,j}+iF^{n-1}_{i,j+1}=0.\tag{24}$$

By putting $k=1$ to arrange the above equation simply,

$$F^{n-1}_{i+1,j}-(1+i)F^{n-1}_{i,j}+iF^{n-1}_{i,j+1}=(1+i)(F^{n}_{i,j}-F^{n-1}_{i,j}).\tag{25}$$

By dividing real and imaginary parts in Eq. (22), we then find that

$$\begin{aligned}\psi_{i+1,j}^{n-1}-\psi_{i,j}^{n-1}+\phi_{i,j}^{n-1}-\phi_{i,j+1}^{n-1}&\\ =\psi_{i,j}^{n}-\psi_{i,j}^{n-1}-(\phi_{i,j}^{n}-\phi_{i,j}^{n-1}),&\\ \psi_{i,j+1}^{n-1}-\psi_{i,j}^{n-1}+\phi_{i+1,j}^{n-1}-\phi_{i,j}^{n-1}&\\ =\psi_{i,j}^{n}-\psi_{i,j}^{n-1}-(\phi_{i,j}^{n}-\phi_{i,j}^{n-1}),&\end{aligned}\tag{26}$$

where $\psi_{i,j}^{n}$, $\phi_{i,j}^{n}$, $\psi_{i,j}^{n-1}$ and $\phi_{i,j}^{n-1}$ are values in other fields of point (i,j).

Let's introduce a new free parameter t, express iterative order by it and deform into the following differential equation.

$$\begin{aligned}\frac{\partial\psi}{\partial x}-\frac{\partial\phi}{\partial y}&=\frac{\partial\psi}{\partial t}-\frac{\partial\phi}{\partial t},\\ \frac{\partial\psi}{\partial y}+\frac{\partial\phi}{\partial x}&=\frac{\partial\psi}{\partial t}+\frac{\partial\phi}{\partial t}.\end{aligned}\tag{27}$$

By introducing the following equations,

$$\psi(x,y,t)=k(t)G(x,y),\qquad \phi(x,y,t)=k(t)H(x,y),\tag{28}$$

and by substituting Eq. (28) into Eq. (27), we then obtain

$$\begin{aligned}k(t)\Big(\frac{\partial G}{\partial x}-\frac{\partial H}{\partial y}\Big)&=\frac{\partial k(t)}{\partial t}(G-H),\\ k(t)\Big(\frac{\partial G}{\partial y}+\frac{\partial H}{\partial x}\Big)&=\frac{\partial k(t)}{\partial t}(G+H).\end{aligned}\tag{29}$$

Then

$$\frac{\left(\frac{\partial G}{\partial x}-\frac{\partial H}{\partial y}\right)}{G-H}=\frac{\left(\frac{\partial G}{\partial y}+\frac{\partial H}{\partial x}\right)}{G+H}=\frac{k'(t)}{k(t)}=-\lambda_m^2.\tag{30}$$

From Eq. (30) we find that

$$k'(t)+\lambda_m^2 k(t)=0.\tag{31}$$

and

$$\begin{aligned}\frac{\partial G}{\partial x}-\frac{\partial H}{\partial y}+\lambda_m^2(G-H)&=0,\\ \frac{\partial G}{\partial y}+\frac{\partial H}{\partial x}+\lambda_m^2(G+H)&=0.\end{aligned}\tag{32}$$

By introducing the following equations,

$$G(x,y)=A(x)B(y),\qquad H(x,y)=C(x)D(y).\tag{33}$$

By substituting Eq. (33) into Eq. (32), we then have

$$\frac{dA}{dx}.\frac{1}{C}+\lambda_m^2\frac{A}{C}=\frac{1}{B}.\frac{dD}{dy}+\lambda_m^2\frac{D}{B}.\tag{34}$$

Because left side and right side of Eq. (34) are functions about x and y, they are constant m.

$$\begin{aligned}\frac{dA}{dx}+\lambda_m^2A-Cm&=0,\\ \frac{dD}{dy}+\lambda_m^2D-Bm&=0.\end{aligned}\tag{35}$$

By substituting Eq. (33) into Eq. (35), Eq. (33) equals as follows:

$$\frac{1}{D}.\frac{dB}{dy}+\lambda_m^2\frac{B}{D}=-\frac{1}{A}.\frac{dC}{dx}-\lambda_m^2\frac{C}{A}.\tag{36}$$

Because left side and right side in Eq. (36) are functions of x and y, they are constant n. Then above equation equals as follows:

$$\begin{aligned}\frac{dB}{dy}+\lambda_m^2B-Dn&=0,\\ \frac{dC}{dx}+\lambda_m^2C+An&=0.\end{aligned}\tag{37}$$

By deciding A, B, C and D from Eqs. (35) and (37), we can decide $G(x,y)$ and $H(x,y)$ from Eq. (33). Thus, we can get ψ and ϕ of Eq. (33).

$$\begin{aligned}\psi(x,y,t)&=G_0(x,y)+\sum_{m=1}^{\infty}A_m e^{-\lambda_m^2 t}G_m(x,y),\\ \phi(x,y,t)&=H_0(x,y)+\sum_{m=1}^{\infty}B_m e^{-\lambda_m^2 t}H_m(x,y).\end{aligned}\tag{38}$$

In Eq. (38), $G_0(x,y)$ and $H_0(x,y)$ are solutions of the following equations

$$\begin{aligned}\frac{\partial G}{\partial x}-\frac{\partial H}{\partial y}&=0,\\ \frac{\partial G}{\partial y}+\frac{\partial H}{\partial x}&=0.\end{aligned}\tag{39}$$

The second term of right side in Eq. (38) is an error of iterative calculation. The value of this term is 0 on $t\to\infty$.

$$\begin{aligned}lim_{t\to\infty}\psi(x,y,t)&=G_0(x,y),\\ lim_{t\to\infty}\phi(x,y,t)&=H_0(x,y).\end{aligned}\tag{40}$$

Thus, the result of simple iterative calculation converges to solution of Cauchy-Riemann differential equations from above result we can know that numerical calculation has convergence. The convergence is decided by power λ_1^2 of the second term in right side of Eq. (38), where λ_1^2 is the smallest eigenvalue. The greater this power is, the higher the convergence is. The above eigenvalue equals λ_1^2nh.

We can see that convergence is inversely proportional to the step size. That is proportional to the total number of grid points. Thus, power represents the convergence of *nth* iterative calculation. Thus, λ_1^2h shows the increment of convergent velocity in the first iterative calculation.

3 Numerical results on the viscous laminar flow in the straight pipe

We have considered the new method of calculating the velocity of Poiseuille flow and Couette flow by using the complex variable finite difference method in this paper. We consider *N-S* equation in order to calculate the steady laminar flow velocity of viscous fluid in the straight pipe,

$$\frac{dV}{dt} = \frac{\partial V}{\partial t} + (\nabla.V)V = K - \frac{1}{\rho} gradP + \gamma.\nabla^2 V. \tag{41}$$

$$\begin{aligned}
&\frac{\partial u}{\partial t} + u\frac{\partial u}{\partial x} + v\frac{\partial u}{\partial y} + w\frac{\partial u}{\partial z} = X - \frac{1}{\rho}.\frac{\partial p}{\partial x} \\
&\qquad + \frac{\mu}{\rho}\left(\frac{\partial^2 u}{\partial x^2} + \frac{\partial^2 u}{\partial y^2} + \frac{\partial^2 u}{\partial z^2}\right), \\
&\frac{\partial v}{\partial t} + u\frac{\partial v}{\partial x} + v\frac{\partial v}{\partial y} + w\frac{\partial v}{\partial z} = Y - \frac{1}{\rho}.\frac{\partial p}{\partial y} \\
&\qquad + \frac{\mu}{\rho}\left(\frac{\partial^2 v}{\partial x^2} + \frac{\partial^2 v}{\partial y^2} + \frac{\partial^2 v}{\partial z^2}\right), \\
&\frac{\partial w}{\partial t} + u\frac{\partial w}{\partial x} + v\frac{\partial w}{\partial y} + w\frac{\partial w}{\partial z} = Z - \frac{1}{\rho}.\frac{\partial p}{\partial z} \\
&\qquad + \frac{\mu}{\rho}\left(\frac{\partial^2 w}{\partial x^2} + \frac{\partial^2 w}{\partial y^2} + \frac{\partial^2 w}{\partial z^2}\right),
\end{aligned} \tag{42}$$

where V is the vector of velocity, γ is the kinematical viscosity $\gamma = \mu/\rho$, μ is the viscosity, ρ is the density of fluid and $K = X\hat{i} + Y\hat{j} + Z\hat{k}$.

We assume that the incompressible fluid with viscosity μ moves along constant direction in the straight pipe with different section (see Fig. 4). We set up z-axis as flow direction, while the velocity of x-axis and y-axis is 0. Thus $\partial w/\partial z = 0$, then w is a function about x and y. By applying the motion equation, we get the following equation.

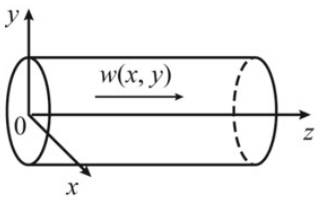

Fig. 4 Flow along z-direction in the straight pipe with different section.

$$\frac{\partial p}{\partial x} = 0, \quad \frac{\partial p}{\partial y} = 0, \quad \frac{\partial p}{\partial z} = \mu\left(\frac{\partial^2 w}{\partial x^2} + \frac{\partial^2 w}{\partial y^2}\right). \tag{43}$$

Here we know that pressure p is only a function of z from first and second equation. Considering the right side of third equation is a function of x and y, we can get a pressure gradient along z-axis in the straight pipe as $\partial p/\partial z = J$ (J is constant). Thus,

$$\frac{\partial^2 w}{\partial x^2} + \frac{\partial^2 w}{\partial y^2} = \frac{J}{\mu}, \tag{44}$$

and we consider that the fluid satisfies the equation $w = 0$ on the wall of pipe. According to it, we can get the distribution of the velocity along x-axis and y-axis,

$$w = \varphi - \frac{J}{4\mu}(x^2 + y^2), \tag{45}$$

where $\varphi(x, y)$ is the harmonic function of satisfying Laplace differential equation. Substituting w into the motion equation, we get the equation about φ.

$$\frac{\partial^2 \varphi}{\partial x^2} + \frac{\partial^2 \varphi}{\partial y^2} = 0. \tag{46}$$

The value of the function satisfying Eq. (46) is expressed as follows:

$$\varphi^2 = \frac{J}{4\mu}(x^2 + y^2). \tag{47}$$

Because the velocity of a Poiseuille flow is 0 on the boundary of the wall, we can calculate the velocity of the steady laminar flow in the straight pipe.

$$w = \varphi - \frac{J}{4\mu}(x^2 + y^2). \tag{48}$$

Therefore, we can get φ by the complex variable finite difference method and then get the velocity w from Eq. (48). Because a pressure gradient along z-axis of Poiseuille flow in the straight pipe is not 0, a pressure gradient along z-axis of Couette flow in the straight pipe is 0. Therefore, the velocity of Poiseuille flow in the straight pipe satisfies a Poisson equation of non-homogeneous second-order partial differential equation. On the other hand, the velocity of Couette flow in the straight pipe satisfies a Laplace equation of the homogeneous second-order partial differential equation.

The approximate velocity of Poiseuille flow and Couette flow in the straight pipe can be easily solved with a computer code made in MATHCAD. Numerical results can be obtained for any straight pipe with a different section, but in order to validate the computer code, we consider a particular case, the problem of approximate velocity of Poiseuille flow and Couette flow in the straight pipe with a rectangular section. It has great importance because it offers us the possibility to make a comparison between the exact solution and the numerical one.

First, we calculate the velocity of Couette flow in the straight pipe by using the present method. The velocity of Couette flow in the straight pipe with rectangular section is represented as a cubic graph. (see Fig. 5) and the different sectional graphics (see Figs. 6, 7 and 8). The width of the rectangular section in the straight pipe is 2400, and

the length of the rectangular section in the straight pipe is 800. The velocities of Couette flow on 4 borders of rectangular section have different sizes respectively, that is, the magnitudes of velocity w on every border are 1000, 2000, 3000 and 4000. After considering the magnitudes of velocity based on the cubic graph, the approximate velocity w of Couette flow in the straight pipe with rectangular section from the calculated results, we can see that the larger the velocity magnitude at the boundary, the larger the cubic gradient of velocity w in the Couette flow in a straight pipe with a rectangular section. Specifically, this paper presents detailed data on the approximate velocities of Couette flow at every section along the width direction. According to this, we can see that the change of velocity of Couette flow from a width of $x = 440$ to $x = 2000$ is not large, and the form of the velocity curves changes very little compared with changes in width.

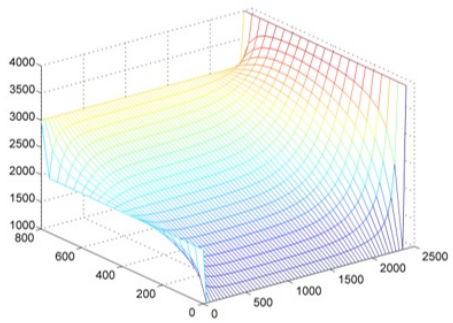

Fig. 5 The approximate velocity w of Couette flow in the straight pipe with rectangular section.

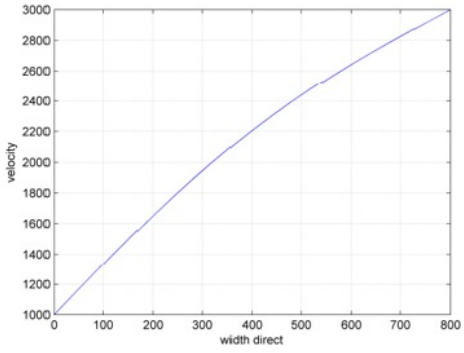

Fig. 6 The approximate velocity w of Couette flow on width $x = 440$ of rectangular section.

Second, we calculate the velocity in Poiseuille flow in a straight pipe using the present method. The size of the velocity w of Poiseuille flow in the straight pipe with rectangular section by the complex variable finite element method is

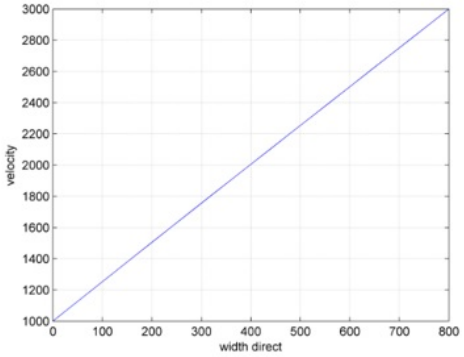

Fig. 7 The approximate velocity w of Couette flow on width $x = 1240$ of rectangular section.

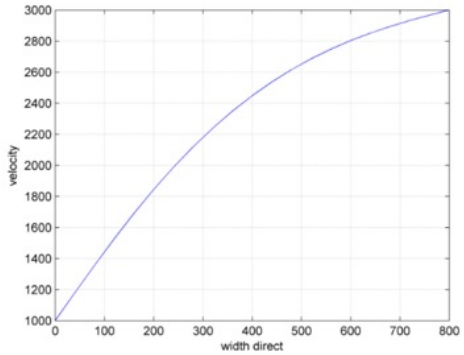

Fig. 8 The approximate velocity w of Couette flow on the width $x = 2000$ of rectangular section.

represented in the cubic graphics (see Fig. 9) and in different sectional graphics respectively (see Figs. 9, 10 and 11). In this paper, we have calculated the velocity w of Poiseuille flow in the straight pipe with rectangular section in the case of pressure gradient $J = \partial p/\partial z = -10$. The width of the rectangular section in the straight pipe is 2400, and the length of the rectangular section in the straight pipe is 800. The velocities of Poiseuille flow on 4 borders of rectangular section have different sizes respectively, that is, the magnitudes of velocity w on every border are 0. After considering the magnitudes of velocity based on the cubic graph of the approximate velocity w of Poiseuille flow in the straight pipe with rectangular section from the calculated results, we can see that the larger the magnitude of velocity on the border, the larger the cubic gradient of velocity w of Poiseuille flow in the straight pipe with rectangular section. Specifically, detailed data on the approximate velocities of Poiseuille flow at every section along the width are presented in this paper. According to this, we can see that the change of velocity of Poiseuille flow from a width of $x = 440$ to $x = 2000$ is not large, and the form of the velocity curves changes very little compared with changes in width. Figs. 10, 11 and 12 show that profiles of velocity curve are reasonably smooth The computational procedure appears to be appropriate for a straight pipe with a different section.

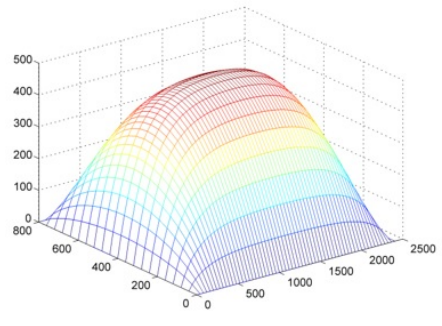

Fig. 9 The approximate velocity w of Poiseuille flow in the straight pipe with rectangular section.

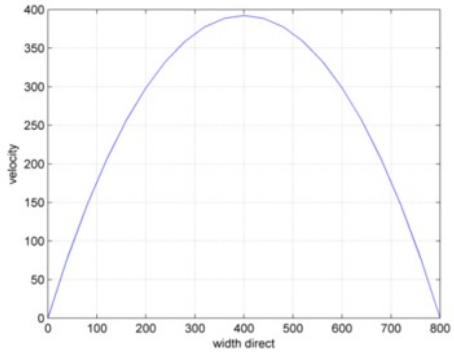

Fig. 10 The approximate velocity w of Poiseuille flow on width $x = 440$ of rectangular section.

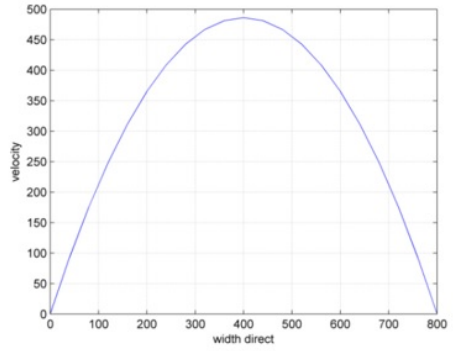

Fig. 11 The approximate velocity w of Poiseuille flow on width $x = 1240$ of rectangular section.

4 Conclusion

In this paper, the complex variable finite difference method (CVFDM) is applied to analyze the viscous laminar flow in a straight pipe. The Cauchy-Riemann differential equation for solving the two-dimensional potential problem is generalized to a complex finite difference equation. To verify the accuracy of the proposed method, the analytical solutions for Poiseuille and Couette flows are obtained.

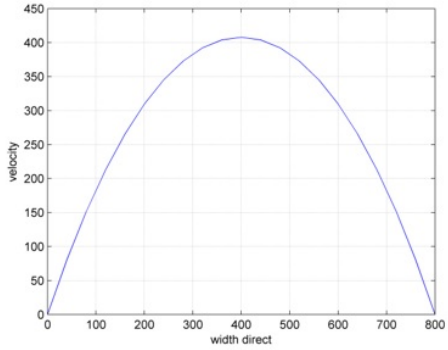

Fig. 12 The approximate velocity w of Poiseuille flow on width $x = 2000$ of rectangular section.

The CVFDM has been demonstrated to be an efficient technique for solving the two-dimensional boundary value problem. The advantages of CVFDM include easy grid generation, fast computation, and high computational accuracy. The CVFEM can also be applied to various physical phenomena that satisfy the Cauchy-Riemann equation.

Declaration of competing interest

The authors declare that they have no conflict of interest.

Funding

This work was supported by ongoing institutional funding. No additional grants to carry out or direct this particular research were obtained.

Author contributions

All authors contribute to the study conception and design. Material preparation, data collection and analysis were performed by Song-Chol Ri, InGu Jo and Namsu Pak. The first draft of the manuscript was written by Song-Chol Ri and all authors commented on previous versions of the manuscript. All authors read and approved the final manuscript.

Acknowledgements The authors would like to express their gratitude to the handling editor and reviewers for their constructive comments.

References

1. T. V. Hromadka, C. Lai, *The complex variable boundary element method in engineering analysis*, (Springer-Verlag, Berlin 1987)
2. M. Mokry, AIAA Journal, **29**, no. 12, 2027 (1991). DOI: https://doi.org/10.2514/3.10836
3. P. C. Dumir, R. Kumar, Appl. Math. Modelling, **17**, 80 (1993). DOI: https://doi.org/10.1016/0307-904X(93)90096-Y

4. K. Sato, Comput. Methods in Appl. Mech. Eng., **192**, 1421 (2003)
5. X. Wang, Whye-Teong Ang, Appl. Math. Comput., **321**, 731 (2018). DOI: https://doi.org/10.1016/j.amc.2017.10.042
6. D. R. Tamayo, A. Montoya, H. Millwater, Eng. Fract. Mech., **192**, 328 (2018). DOI: https://doi.org/10.1016/j.engfracmech.2017.12.013
7. H. Millwater, D. Wagner, A. Montoya, Eng. Fract. Mech., **162**, 95 (2016). DOI: https://doi.org/10.1016/j.engfracmech.2016.04.002
8. R. Fielder, A. Montoya, H. Millwater, P. Golden, Int. J. Mech. Sci., **133**, 112 (2017). DOI: https://doi.org/10.1016/j.ijmecsci.2017.08.035
9. D. Restrepo, et al., Appl. Sci., **12**, no 5, 2738 (2022). DOI: https://doi.org/10.3390/app12052738
10. H. Millwater, et al., Int. J. Solids Struct., **243**, 111545 (2022). DOI: https://doi.org/10.1016/j.ijsolstr.2022.111545
11. G. A. Rios, J. S. R. Tabares, A. Montoya, D. Restrepo, H. Millwater, J. Therm. Stress., **45**, no 5, 341 (2022). DOI: https://doi.org/10.1080/01495739.2022.2034976

TTMP vol 3 (1), 2026
doi: 10.30511/TTMP.2026.2083532.1071

Transactions in Theoretical and Mathematical Physics

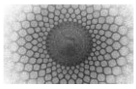

Multiplicity of Homoclinic Solutions for Homogeneous Damped Vibration Systems

Mohsen TIMOUMI[1,a]

[1] Dpt. of Mathematics, Faculty of Sciences, 5000 Monastir, Tunisia.

Received: 09 January 2026 / Accepted: 22 February 2026 / Published: 23 February 2026

Abstract. We study the existence and multiplicity of classical homoclinic solutions for a class of second-order damped vibration systems of the form

$$\ddot{u}(t)+q(t)\dot{u}(t)-L(t)u(t)=-a(t)\nabla G(u(t)) \\ +b(t)\nabla H(u(t))+h(t), \qquad t\in\mathbb{R}.$$

where $L(t)$ is a symmetric positive definite matrix, $a(t), b(t)$ are positive functions, G and H are homogeneous potentials of different degrees, and $h(t)$ is a small external forcing term. Employing variational techniques and the Pohozaev fibering method, we establish the existence of infinitely many nontrivial homoclinic solutions in the symmetric case $h=0$, and at least three such solutions when h is nonzero but sufficiently small. These results generalize previous findings by addressing both subcritical and supercritical homogeneous nonlinearities in a non-periodic, non-symmetric framework.

Keywords. Damped vibration systems, homogeneous functions, variational techniques, Pohozaev fibering method, implicit functions theorem.

1 Introduction

This paper is devoted to the study of the existence and multiplicity of fast homoclinic solutions (see Definition 2.1) for a class of second-order damped vibration systems described by the equation:

$$\ddot{u}(t)+q(t)\dot{u}(t)-L(t)u(t)+\nabla W(t,u(t))=0, \\ \forall t\in\mathbb{R}. \tag{1}$$

where $q:\mathbb{R}\to\mathbb{R}$ is continuous, $L\in C(\mathbb{R},\mathbb{R}^{N^2})$ is symmetric and positive definite for each t, and $W:\mathbb{R}\times\mathbb{R}^N\to\mathbb{R}$ is continuously differentiable with respect to the second variable. A function u is called a classical homoclinic solution to zero of system (1) if $u\in C^2(\mathbb{R},\mathbb{R}^N)$ and satisfies $u(t)\to 0$ and $\dot{u}(t)\to 0$ as $|t|\to\infty$. Such a solution is said to be nontrivial if $u\neq 0$.

When $q=0$, the system reduces to the well-known second-order Hamiltonian system:

$$\ddot{u}(t)-L(t)u(t)+\nabla W(t,u(t))=0,\ \forall t\in\mathbb{R}. \tag{2}$$

which has been extensively studied using variational methods, particularly in the context of autonomous or time-periodic systems (e.g., [1–6]). In such cases, standard compactness arguments and critical point theorems such as the Mountain Pass Theorem are applicable. However, for non-periodic systems where $L(t)$ and $W(t,x)$ do not exhibit temporal periodicity, the lack of compactness due to the unboundedness of time introduces significant analytical challenges. To address these, several authors (e.g., [7**?** –19]) have imposed coercivity or asymptotic growth conditions on $L(t)$ and subcritical or asymptotically linear constraints on the potential W.

In contrast, the damped case $q\neq 0$, which represents more realistic models of vibrating systems subject to energy dissipation, has received comparatively less attention (see [20**? ? ?** –25]). Some works, such as [23**?**], successfully establish the existence of infinitely many fast homoclinic solutions for superquadratic damped systems using variational techniques and compactness assumptions tailored to the properties of $L(t)$. However, most of these contributions are restricted to even or symmetric nonlinearities and do not adequately explore multiplicity in the presence of non-symmetric or non-periodic structures.

[a]e-mail: mtimoumi12@gmail.com

The present work aims to broaden this research direction by considering damped systems governed by a non-periodic potential of the form:

$$W(t,x) = -a(t)G(x) + b(t)H(x) + h(t)\cdot x. \tag{3}$$

where G and H are homogeneous functions of degrees ν and μ, respectively, with $1 < \nu < \mu$, and $h(t)$ is a small external forcing term. This setting allows the inclusion of both subcritical and supercritical nonlinearities, thus extending prior results to a more general and physically relevant class of systems. Importantly, we do not impose periodicity or evenness assumptions on the potentials, making the problem non-symmetric and non-autonomous. Our approach is based on the Pohozaev fibering method [**? ?**] and variational techniques developed in [23], combined with a measure-theoretic condition on $L(t)$ that ensures a suitable form of compactness:
There exists a positive constant r_0 such that $\inf_{t\in\mathbb{R}} \inf_{|\xi|=1} L(t)\xi\cdot\xi > 0$ and

$$\lim_{|s|\to\infty} \operatorname{meas}\{t \in (s-r_0, s+r_0) : L(t) \leq MI_N\} = 0, \quad \forall M > 0. \tag{4}$$

Under these settings, we establish the following main results. We impose the following assumptions on the functions a, b, G, H:

Under these settings, we establish the following main results. We impose the following assumptions on the functions a, b, G, H:

(W_1) $G, H \in C^1(\mathbb{R}^N, \mathbb{R})$ and there exist constants ν, μ with $1 < \nu \leq 2 < \mu$ such that $G(sx) = |s|^\nu G(x)$ and $H(sx) = |s|^\mu H(x)$ for all $(s,x) \in \mathbb{R}\times\mathbb{R}^N$.

(W_2) $G(x) > 0$ and $H(x) > 0$ for all $|x| = 1$.

(W_3) $a \in C(\mathbb{R}, \mathbb{R}^+)$, with a bounded if $\nu \geq 2$, and $a \in L^{\frac{2}{2-\nu}}(\mathbb{R})$ if $1 < \nu < 2$.

(W_4) $b \in C(\mathbb{R}, \mathbb{R}^+)$ is bounded.

Theorem 1.1. (Symmetric Case). Let $h = 0$. Assume that conditions (4) and $(W_1) - (W_4)$ hold. Then system (1) admits infinitely many nontrivial fast homoclinic solutions.

Remark 1.1. This result generalizes the multiplicity results obtained in [23] by accommodating potentials that combine both subcritical and supercritical homogeneous components, and by removing the requirement of symmetry.

Theorem 1.2. (Non-Symmetric Case). Let $h \in L_Q^{\mu'}(\mathbb{R}, \mathbb{R}^N)$, where $\frac{1}{\mu} + \frac{1}{\mu'} = 1$. Suppose that assumptions (4) and $(W_1) - (W_4)$ hold. Then there exists a constant $\delta > 0$ such that if $\|h\|_{L_Q^{\mu'}} < \delta$, the system (1) possesses at least three nontrivial fast homoclinic solutions.

Remark 1.2. This significantly extends earlier multiplicity results for the Hamiltonian case (see [13, 16]) to damped, non-symmetric systems, demonstrating robustness of the variational approach even under non-periodic perturbations.

To the best of our knowledge, this is the first study to address multiplicity of fast homoclinic solutions in damped systems governed by non-periodic combinations of homogeneous potentials without imposing symmetry or periodicity. These results therefore provide a meaningful extension of the existing theory and open new directions in the variational analysis of dissipative mechanical systems with complex nonlinear structures.

The structure of this paper is as follows: Section 2 presents some preliminary results and revisits the Pohozaev fibering method. Section 3 is focused on proving Theorem 1.1, while Section 4 addresses the proof of Theorem 1.2.

2 Preliminaries

In order to introduce the concept of fast homoclinic solutions for (1) conveniently, we firstly describe some properties of the weighted Sobolev space E on which the certain variational functional associated with (1) is defined and the fast homoclinic solutions of (1) are the critical points of such functional. Let $Q(t) = \int_0^t q(s)ds$, we shall use $L_Q^2(\mathbb{R})$ to denote the Hilbert space of measurable functions from $\mathbb{R}$ into $\mathbb{R}^N$ under the inner product We define the weighted inner product

$$\langle u, v\rangle_{L_Q^2} = \int_{\mathbb{R}} e^{Q(t)}\, u(t)\cdot v(t)\, dt, \tag{5}$$

and the induced norm

$$\|u\|_{L_Q^2} = \Big(\int_{\mathbb{R}} e^{Q(t)}|u(t)|^2 dt\Big)^{\frac{1}{2}}. \tag{6}$$

Similarly, for $1 \leq s < \infty$, $L_Q^s(\mathbb{R})$ denotes the Banach space of $\mathbb{R}^N$-valued functions on $\mathbb{R}$ with norm

$$\|u\|_{L_Q^s} = \Big(\int_{\mathbb{R}} e^{Q(t)}|u(t)|^s dt\Big)^{\frac{1}{s}}, \tag{7}$$

while $L_Q^\infty(\mathbb{R})$ is endowed with the norm

$$\|u\|_{L_Q^\infty} = \operatorname*{ess\,sup}_{t\in\mathbb{R}} \big(e^{\frac{Q(t)}{2}}|u(t)|\big). \tag{8}$$

In this section, we assume that L satisfies (4) and introduce the Hilbert space

$$E = \Big\{u \in H_Q^1(\mathbb{R}) : \int_{\mathbb{R}} e^{Q(t)} L(t)u(t)\cdot u(t)\, dt < \infty\Big\}. \tag{9}$$

equipped with the following inner product

$$\langle u,v\rangle = \int_{\mathbb{R}} e^{Q(t)}\big(\dot{u}(t)\cdot\dot{v}(t)+L(t)u(t)\cdot v(t)\big)\,dt, \tag{10}$$

and the induced norm $\|u\| = \langle u,u\rangle^{1/2}$. Here, $H^1_Q(\mathbb{R})$ denotes the Sobolev space

$$H^1_Q(\mathbb{R}) = \big\{u\in L^2_Q(\mathbb{R}) : \dot{u}\in L^2_Q(\mathbb{R})\big\}. \tag{11}$$

Evidently, E is continuously embedded into $L^s_Q(\mathbb{R})$ for $2\le s\le\infty$, i.e., for all $2\le s\le\infty$, there exists a constant $\eta_s>0$ such that

$$\|u\|_{L^s_Q} \le \eta_s\|u\|, \ \forall u\in E. \tag{12}$$

Definition 2.1. A solution u of (1) is called a fast homoclinic solution if $u\in E$.

Lemma 2.1. [23] Assume that (4) are satisfied. Then E is compactly embedded in $L^s_Q(\mathbb{R})$ for all $2\le s<\infty$.

To prove our results, we will employ the spherical fibering method as introduced by Pohozaev in [**? ?**]. For the sake of completeness, we will recall this method here. Consider a real Banach space X with a norm $\|u\|_X$ that is differentiable for $u\neq 0$. Let I be a functional on X of class $C^1(X\setminus\{0\})$. We can associate I with a functional $\widetilde{I}$ defined on $\mathbb{R}\times X$ as follows:

$$\widetilde{I}(t,v) = I(tv), \quad \forall (t,v)\in\mathbb{R}\times X. \tag{13}$$

Let S denote the unit sphere in X. The following result holds:

Theorem 2.1. Let X be a real Banach space with a norm differentiable on $X\setminus\{0\}$, and let $(t,v)\in(\mathbb{R}\setminus\{0\})\times S$ be a conditionally critical point of the functional $\widetilde{I}$ considered on $\mathbb{R}\times S$. Then the vector $u=tv$ is a critical point of the functional I, that is, $I'(u)=0$. In other words, any critical point (t,v) of $\widetilde{I}$ restricted on $(\mathbb{R}\setminus\{0\})\times S$ generates the free nontrivial critical point u of I and vice-versa, that is, the problem $I'(u)=0, u\neq 0$ is equivalent to

$$\begin{cases}\widetilde{I}'_t(t,v)=0,\\ \widetilde{I}'_v(t,v)=0.\end{cases} \tag{14}$$

for $\|v\|=1$. In the following, we will call the first scalar system of the previous system the "bifurcation system".

3 Proof of Theorem 1.1.

We will proceed by successive lemmas.

Lemma 3.1. Let $K:\mathbb{R}^N\to\mathbb{R}$ be a function and $\beta>0$ be a constant. We have the following properties:
a) Equivalence of Homogeneity and Evenness: K is homogeneous of degree β if and only if K is even and positively homogeneous of degree β.
b) Bounds on Positively Homogeneous Functions: If K is positively homogeneous of degree β, then there exist constants $m_K, M_K\in\mathbb{R}$ such that

$$m_K|x|^\beta \le K(x) \le M_K|x|^\beta, \quad \forall x\in\mathbb{R}^N. \tag{15}$$

c) Derivative of Positively Homogeneous Functions: If K is differentiable and positively homogeneous of degree β, then ∇K is positively homogeneous of degree $\beta-1$. Furthermore, for all $x\in\mathbb{R}^N$, the following identity holds:

$$\nabla K(x)\cdot x = \beta K(x). \tag{16}$$

Proof **(a)** It suffices to observe that

$$K(-x) = K((-1)x) = |-1|^\beta K(x) = K(x). \tag{17}$$

(b) For $x\in\mathbb{R}^N\setminus\{0\}$, we have

$$K(x) = K\left(|x|\frac{x}{|x|}\right) = |x|^\beta K\left(\frac{x}{|x|}\right). \tag{18}$$

Let

$$m_K = \min_{\{|x|=1\}} K(x), \quad M_K = \max_{\{|x|=1\}} K(x), \tag{19}$$

then

$$m_K|x|^\beta \le K(x) \le M_K|x|^\beta, \quad \forall x\in\mathbb{R}^N. \tag{20}$$

(c) For $s>0$ and any $y\in\mathbb{R}^N$,

$$\begin{aligned}\nabla K(sx)\cdot y &= \lim_{t\to 0^+}\frac{K(sx+ty)-K(sx)}{t}\\ &= \lim_{t\to 0^+} s^{\beta-1}\frac{K\big(x+\frac{t}{s}y\big)-K(x)}{t/s}\\ &= s^{\beta-1}\nabla K(x)\cdot y.\end{aligned} \tag{21}$$

Since y is arbitrary, it follows that $\nabla K(sx) = s^{\beta-1}\nabla K(x)$. Differentiating

$$K(sx) = s^\beta K(x), \tag{22}$$

with respect to s, we obtain

$$\nabla K(sx)\cdot x = \beta s^{\beta-1}K(x). \tag{23}$$

Setting $s=1$ yields the desired result.

Lemma 3.2. Assume that $(W_1)-(W_4)$ are satisfied. Then, we have

a) If $u_n \to u$ in $L_Q^2(\mathbb{R})$, then $a\nabla G(u_n) \to a\nabla G(u)$ in $L_Q^2(\mathbb{R})$.

b) If $u_n \to u$ in $L_Q^\mu(\mathbb{R})$, then $a\nabla H(u_n) \to a\nabla H(u)$ in $L_Q^{\frac{\mu}{\mu-1}}(\mathbb{R})$.

Proof: **a)** If $u_n \to u$ in $L_Q^2(\mathbb{R})$. We claim that $a\nabla G(u_n) \to a\nabla G(u)$ in $L_Q^2(\mathbb{R})$. Arguing indirectly that there exist a subsequence (u_{n_k}) and a constant $\varepsilon_0 > 0$ such that

$$\int_{\mathbb{R}} e^{Q(t)} a^2(t) \big|\nabla G(u_{n_k}(t)) - \nabla G(u(t))\big|^2 dt \geq \varepsilon_0, \quad \forall k \in \mathbb{N}. \tag{24}$$

Up to a subsequence if necessary, we can assume that $\sum_{k=1}^{\infty} \|u_{n_k} - u\|_{L_Q^2} < \infty$ and $u_{n_k} \to u$ a.e. on $\mathbb{R}$. Let $v(t) = \sum_1^\infty |u_{n_k}(t) - u(t)|$, then $v \in L_Q^2(\mathbb{R})$ and we have

$$\begin{aligned}
&a^2(t)\,|\nabla G(u_{n_k}(t)) - \nabla G(u(t))|^2 \\
&\leq a^2(t) M_{|\nabla G|}^2 \big(|u_{n_k}(t)|^{\nu-1} + |u(t)|^{\nu-1}\big)^2 \\
&\leq 2a^2(t) M_{|\nabla G|}^2 \big(|u_{n_k}(t)|^{2(\nu-1)} + |u(t)|^{2(\nu-1)}\big) \\
&\leq 2a^2(t) M_{|\nabla G|}^2 \big((|u_{n_k}(t) - u(t)| + |u(t)|)^{2(\nu-1)} \\
&\qquad + |u(t)|^{2(\nu-1)}\big) \\
&\leq c_1 a^2(t) \big(v^{2(\nu-1)}(t) + |u(t)|^{2(\nu-1)}\big) = w(t).
\end{aligned} \tag{25}$$

where c_1 is a positive constant. By (W_3), $w \in L_Q^1(\mathbb{R})$, hence by the dominated convergence theorem, one gets

$$\int_{\mathbb{R}} e^{Q(t)} a^2(t)\,|\nabla G(u_{n_k}(t)) - \nabla G(u(t))|^2 \, dt \to 0, \quad k \to \infty. \tag{26}$$

which contradicts (24). Hence $a\nabla G(u_n) \to a\nabla G(u)$ in $L_Q^2(\mathbb{R})$.

b) Let $u_n \to u$ in $L_Q^\mu(\mathbb{R})$. We claim that $b\nabla H(u_n) \to b\nabla H(u)$ in $L_Q^{\frac{\mu}{\mu-1}}(\mathbb{R})$. Arguing indirectly that there exist a subsequence (u_{n_k}) and a constant $\varepsilon_0 > 0$ such that

$$\int_{\mathbb{R}} e^{Q(t)} b^{\frac{\mu}{\mu-1}}(t) |\nabla H(u_{n_k}(t)) - \nabla H(u(t))|^{\frac{\mu}{\mu-1}} \, dt \geq \varepsilon_0, \quad \forall k \in \mathbb{N}. \tag{27}$$

Taking a subsequence if necessary, we can assume that $\sum_1^\infty \|u_{n_k} - u\|_{L_Q^\mu} < \infty$ and $u_{n_k} \to u$ a.e. on $\mathbb{R}$. Let $v(t) = \sum_1^\infty |u_{n_k}(t) - u(t)|$, then $v \in L_Q^\mu(\mathbb{R})$ and we have

$$\begin{aligned}
&b^{\frac{\mu}{\mu-1}}(t) |\nabla H(u_{n_k}(t)) - \nabla H(u(t))|^{\frac{\mu}{\mu-1}} \\
&\leq b^{\frac{\mu}{\mu-1}}(t) M_{\nabla H}^{\frac{\mu}{\mu-1}} \big(|u_{n_k}(t)|^{\mu-1} + |u(t)|^{\mu-1}\big)^{\frac{\mu}{\mu-1}} \\
&\leq 2^{\frac{1}{\mu-1}} b^{\frac{\mu}{\mu-1}}(t) M_{\nabla H}^{\frac{\mu}{\mu-1}} \big(|u_{n_k}(t)|^{\mu} + |u(t)|^{\mu}\big) \\
&\leq 2^{\frac{1}{\mu-1}} b^{\frac{\mu}{\mu-1}}(t) M_{\nabla H}^{\frac{\mu}{\mu-1}} \big((|u_{n_k}(t) - u(t)| + |u(t)|)^{\mu} \\
&\qquad + |u(t)|^{\mu}\big) \\
&\leq c_2 \big(v^\mu(t) + |u(t)|^\mu\big) = w(t).
\end{aligned} \tag{28}$$

where c_2 is a positive constant. Since $w \in L_Q^1(\mathbb{R})$, then by the dominated convergence theorem, one gets

$$\int_{\mathbb{R}} e^{Q(t)} b^{\frac{\mu}{\mu-1}}(t) |\nabla H(u_{n_k}(t)) - \nabla H(u(t))|^{\frac{\mu}{\mu-1}} \, dt \to 0, \quad k \to \infty, \tag{29}$$

which contradicts (27). Hence the claim is verified. ∎

Lemma 3.3. Assume that $(W_1)-(W_3)$ are satisfied. Then the functionals

$$I_1(u) = \int_{\mathbb{R}} e^{Q(t)} a(t) G(u(t))\, dt, \tag{30}$$

$$I_2(u) = \int_{\mathbb{R}} e^{Q(t)} b(t) H(u(t))\, dt, \tag{31}$$

are continuously differentiable respectively on $L_Q^2(\mathbb{R})$ and $L_Q^\mu(\mathbb{R})$, and we have

$$I_1'(u)v = \int_{\mathbb{R}} e^{Q(t)} a(t) \nabla G(u(t)) \cdot v(t)\, dt, \quad \forall u, v \in L_Q^2(\mathbb{R}), \tag{32}$$

$$I_2'(u)v = \int_{\mathbb{R}} e^{Q(t)} b(t) \nabla H(u(t)) \cdot v(t)\, dt, \quad \forall u, v \in L_Q^\mu(\mathbb{R}). \tag{33}$$

Proof: **a)** For $u, v \in L_Q^2(\mathbb{R})$, by the Mean Value Theorem and Hölder's inequality, we have

$$\begin{aligned}
&\big|I_1(u+v) - I_1(u) \\
&\quad - \int_{\mathbb{R}} e^{Q(t)} a(t) \nabla G(u(t)) \cdot v(t)\, dt\big| \\
&= \Big| \int_{\mathbb{R}} e^{Q(t)} a(t) \big[G(u(t)+v(t)) - G(u(t)) \\
&\qquad - \nabla G(u(t)) \cdot v(t)\big] dt \Big| \\
&= \Big| \int_{\mathbb{R}} e^{Q(t)} a(t) \big[\nabla G(u(t) + \theta(t) v(t)) \\
&\qquad - \nabla G(u(t))\big] \cdot v(t)\, dt \Big| \\
&\leq \Big(\int_{\mathbb{R}} e^{Q(t)} a^2(t) |\nabla G(u(t) + \theta(t) v(t)) \\
&\qquad - \nabla G(u(t))|^2 dt \Big)^{1/2} \|v\|_{L_Q^2}.
\end{aligned} \tag{34}$$

where $\theta(t) \in]0,1[$. By Lemma 3.2, the functional defined on $L^2_Q(\mathbb{R})$ by

$$v \mapsto \int_{\mathbb{R}} e^{Q(t)} a^2(t) |\nabla G(u(t)+v(t)) - \nabla G(u(t))|^2 dt \tag{35}$$

goes to zero as $v \to 0$. Hence

$$\begin{aligned} &I_1(u+v) - I_1(u) \\ &\quad - \int_{\mathbb{R}} e^{Q(t)} a(t) \nabla G(u(t)) \cdot v(t)\, dt \\ &= o(\|v\|_{L^2_Q}). \end{aligned} \tag{36}$$

Thus I_1 is differentiable at u and

$$I_1'(u)v = \int_{\mathbb{R}} e^{Q(t)} a(t) \nabla G(u(t)) \cdot v(t)\, dt. \tag{37}$$

Let $u_n \to u$ in $L^2_Q(\mathbb{R})$. Then

$$\begin{aligned} \|I_1'(u_n) - I_1'(u)\| &= \sup_{\|v\|_{L^2_Q}=1} \Big| \int_{\mathbb{R}} e^{Q(t)} a(t) \\ &\qquad \times [\nabla G(u_n(t)) - \nabla G(u(t))] \cdot v(t)\, dt \Big| \\ &\le \Big(\int_{\mathbb{R}} e^{Q(t)} a^2(t) |\nabla G(u_n(t)) - \nabla G(u(t))|^2 dt \Big)^{1/2} \\ &\to 0, \quad n \to \infty. \end{aligned} \tag{38}$$

Hence I_1 is continuously differentiable on $L^2_Q(\mathbb{R})$.

b) For $u, v \in L^\mu_Q(\mathbb{R})$, by the Mean Value Theorem and Hölder's inequality, we have

$$\begin{aligned} &\big| I_2(u+v) - I_2(u) \\ &\quad - \int_{\mathbb{R}} e^{Q(t)} b(t) \nabla H(u(t)) \cdot v(t)\, dt \big| \\ &= \Big| \int_{\mathbb{R}} e^{Q(t)} b(t) \big[H(u(t)+v(t)) - H(u(t)) \\ &\qquad - \nabla H(u(t)) \cdot v(t) \big] dt \Big| \\ &= \Big| \int_{\mathbb{R}} e^{Q(t)} b(t) \big[\nabla H(u(t)+\theta(t)v(t)) \\ &\qquad - \nabla H(u(t)) \big] \cdot v(t)\, dt \Big| \\ &\le M_b \Big(\int_{\mathbb{R}} e^{Q(t)} |\nabla H(u(t)+\theta(t)v(t)) \\ &\qquad - \nabla H(u(t))|^{\frac{\mu}{\mu-1}} dt \Big)^{\frac{\mu-1}{\mu}} \|v\|_{L^\mu_Q}. \end{aligned} \tag{39}$$

where $\theta(t) \in (0,1)$. By Lemma 3.2, $\int_{\mathbb{R}} e^{Q(t)} |\nabla H(u(t)+v(t)) - \nabla H(u(t))|^{\frac{\mu}{\mu-1}} dt \to 0$ as $v \to 0$. Hence

$$\begin{aligned} &I_2(u+v) - I_2(u) \\ &\quad - \int_{\mathbb{R}} e^{Q(t)} b(t) \nabla H(u(t)) \cdot v(t)\, dt = o(\|v\|_{L^\mu_Q}). \end{aligned} \tag{40}$$

Thus I_2 is differentiable on $L^\mu_Q(\mathbb{R})$ and $I_2 \in C^1(L^\mu_Q(\mathbb{R}))$. The proof of Lemma 3.3 is completed. ∎

Remark 3.1. Using Lemmas 2.2, 3.3, it is easy to see that I_1 and I_2 are continuously differentiable on E.

Associated to system (1), is the energy functional $J_0 : E \to \mathbb{R}$ defined by

$$\begin{aligned} J_0(u) &= \frac{1}{2} \int_{\mathbb{R}} e^{Q(t)} \big(|\dot{u}(t)|^2 + L(t)u(t) \cdot u(t) \big)\, dt \\ &\quad - \int_{\mathbb{R}} e^{Q(t)} W(t, u(t))\, dt \\ &= \frac{1}{2} \|u\|^2 + \int_{\mathbb{R}} e^{Q(t)} a(t) G(u(t))\, dt \\ &\quad - \int_{\mathbb{R}} e^{Q(t)} b(t) H(u(t))\, dt. \end{aligned} \tag{41}$$

From Remark 3.1, J_0 is continuously differentiable on E with derivative

$$\begin{aligned} J_0'(u)v &= \int_{\mathbb{R}} e^{Q(t)} \dot{u}(t) \cdot \dot{v}(t)\, dt \\ &\quad + \int_{\mathbb{R}} e^{Q(t)} L(t)u(t) \cdot v(t)\, dt \\ &\quad + \int_{\mathbb{R}} e^{Q(t)} a(t) \nabla G(u(t)) \cdot v(t)\, dt \\ &\quad - \int_{\mathbb{R}} e^{Q(t)} b(t) \nabla H(u(t)) \cdot v(t)\, dt. \end{aligned} \tag{42}$$

for all $u, v \in E$. Moreover, the critical points of J_0 on E correspond to the solutions of (1).

According to the spherical fibering method, we look for critical points of the form

$$u = sv, \quad s \in \mathbb{R},\ v \in E,\ \|v\| = 1. \tag{43}$$

The functional J_0 extends to $\mathbb{R} \times E$ by

$$\begin{aligned} \widetilde{J}_0(s,v) &= J_0(sv) \\ &= \frac{s^2}{2} \|v\|^2 + \int_{\mathbb{R}} e^{Q(t)} a(t) G(sv(t)) dt \\ &\quad - \int_{\mathbb{R}} e^{Q(t)} b(t) H(sv(t)) dt \\ &= \frac{s^2}{2} \|v\|^2 + |s|^\nu \int_{\mathbb{R}} e^{Q(t)} a(t) G(v(t)) dt \\ &\quad - |s|^\mu \int_{\mathbb{R}} e^{Q(t)} b(t) H(v(t)) dt, \end{aligned} \tag{44}$$

for $(s,v) \in \mathbb{R} \times E$.

Its restriction to $\mathbb{R} \times S$, with $S = \{v \in E : \|v\| = 1\}$, reads

$$\widetilde{J}_0(s,v) = \frac{s^2}{2} + |s|^\nu \int_{\mathbb{R}} e^Q a G(v) - |s|^\mu \int_{\mathbb{R}} e^Q b H(v). \tag{45}$$

If $s \neq 0$, the bifurcation equation $\partial_s \widetilde{J}_0(s,v) = 0$ becomes

$$\begin{aligned} &s + \nu |s|^{\nu-2} s \int_{\mathbb{R}} e^{Q(t)} a(t) G(v(t)) dt \\ &\quad - \mu |s|^{\mu-2} s \int_{\mathbb{R}} e^{Q(t)} b(t) H(v(t)) dt = 0, \end{aligned} \tag{46}$$

which is equivalent to

$$\begin{aligned} &1+\nu|s|^{\nu-2}\int_{\mathbb{R}} e^{Q(t)}a(t)G(v(t))dt \\ &-\mu|s|^{\mu-2}\int_{\mathbb{R}} e^{Q(t)}b(t)H(v(t))dt=0. \end{aligned} \tag{47}$$

Lemma 3.4. For any $v\in\widetilde{E}=L^2_Q(\mathbb{R})\cap L^\mu_Q(\mathbb{R})$, the function

$$\begin{aligned} \varphi_v(s)=1+\nu|s|^{\nu-2}&\int_{\mathbb{R}} e^{Q(t)}a(t)G(v(t))\,dt \\ &-\mu|s|^{\mu-2}\int_{\mathbb{R}} e^{Q(t)}b(t)H(v(t))\,dt. \end{aligned} \tag{48}$$

possesses exactly two zeros $\pm s(v)$. Moreover, the functional $v\mapsto s(v)$ is continuously differentiable on $\widetilde{E}$.

Proof : Since $1<\nu\le\max\{2,\nu\}<\mu$, then it is clear that

$$\lim_{|s|\to\infty}\varphi_v(s)=-\infty. \tag{49}$$

Moreover

$$\lim_{s\to0^+}\varphi_v(s)= \begin{cases} +\infty, & 1<\nu<2,\\ 1+\nu\displaystyle\int_{\mathbb{R}} e^{Q(t)}a(t)G(v(t))\,dt, & \nu=2,\\ 1, & \nu>2. \end{cases} \tag{50}$$

Since φ_v is continuous, we deduce by the Mean Value Theorem that φ_v has at least two zeros. It remains to prove that φ_v has exactly two zeros. Indeed, for $s\neq0$, we have

$$\begin{aligned} \varphi_v'(s)=\nu(\nu-2)|s|^{\nu-4}s&\int_{\mathbb{R}} e^{Q(t)}a(t)G(v(t))\,dt \\ &-\mu(\mu-2)|s|^{\mu-4}s\int_{\mathbb{R}} e^{Q(t)}b(t)H(v(t))\,dt. \end{aligned} \tag{51}$$

We discuss two cases.
a) First case: $1<\nu\le2$, φ_v' does not admit zeros. Hence φ_v has exactly two zeros: $\pm s(v)$.
b) Second case: $\nu>2$. In this case, φ_v' possesses two zeros $\pm\overline{s}(v)$ with

$$\overline{s}(v)=\left(\frac{\nu(\nu-2)\int_{\mathbb{R}} e^{Q(t)}a(t)G(v(t))\,dt}{\mu(\mu-2)\int_{\mathbb{R}} e^{Q(t)}b(t)H(v(t))\,dt}\right)^{\frac{1}{\mu-\nu}}. \tag{52}$$

Using the variation table, we see directly that φ_v admits exactly two zeros $\pm s(v)$ with $s(v)>\overline{s}(v)$.
Now, we shall prove that the functional $v\mapsto s(v)$ obtained above is continuously differentiable on $\widetilde{E}$. Let $v_0\in\widetilde{E}$, we consider the functional $\Phi:\widetilde{E}\times I\to\mathbb{R}$ defined by $\Phi(v,s)=\varphi_v(s)$, where $I=\mathbb{R}_+^*$ if $1<\nu\le2$ and $I=]\overline{s}(v),+\infty[$ if $\nu>2$. Lemma 3.3 implies that Φ is continuously differentiable on $\widetilde{E}\times I$. Moreover, we have $\Phi(v_0,s(v_0))=0$ and $\frac{\partial\Phi}{\partial s}(v_0,s(v_0))\neq0$. By the Implicit Function Theorem, there exist an open neighborhood $V\subset\widetilde{E}$ of v_0 and a unique $\theta:V\to\mathbb{R}$ which is continuously differentiable such that $\Phi(v,\theta(v))=0,\quad\forall v\in V$. By the uniqueness of s and θ, we deduce that $s=\theta$ on V, so s is continuously differentiable on V and in particular at v_0. Since v_0 is arbitrary, then s is continuously differentiable on $\widetilde{E}$.
Now, consider the functional $\widehat{J}_0$ defined on $\widetilde{E}$ by

$$\begin{aligned} \widehat{J}_0(v)=\frac{1}{2}s^2(v)+|s(v)|^\nu&\int_{\mathbb{R}} e^{Q(t)}a(t)G(v(t))\,dt \\ &-|s(v)|^\mu\int_{\mathbb{R}} e^{Q(t)}b(t)H(v(t))\,dt. \end{aligned} \tag{53}$$

for $v\in\widetilde{E}$. We deduce from Lemmas 3.3, 3.4 that $\widehat{J}_0(v)=\widetilde{J}_0(s(v),v)$ on S. From system $\varphi_v(s(v))=0$, we deduce that for all $v\in S$

$$\begin{aligned} \widehat{J}_0(v)=\left(\tfrac{1}{2}-\tfrac{1}{\mu}\right)&s^2(v) \\ &+\nu\left(\tfrac{1}{\nu}-\tfrac{1}{\mu}\right)|s(v)|^\nu\int_{\mathbb{R}} e^{Q(t)}a(t)G(v(t))\,dt. \end{aligned} \tag{54}$$

Since $1<\nu\le\max\{2,\nu\}<\mu$, $b\ge0$ and $G\ge0$, then $\widehat{J}_0$ is bounded from below on S as the sum of two non-negative terms. Let $(v_n)\subset S$ be such that $\widehat{J}_0(v_n)\to\inf_{v\in S}\widehat{J}_0(v)$. Since (v_n) is bounded, then up to a subsequence, we can assume that $v_n\rightharpoonup\overline{v}$ weakly in E. By Theorem 2.1, we can assume after going to a subsequence, that $v_n\to\overline{v}$ in both $L^2_Q(\mathbb{R})$ and $L^\mu_Q(\mathbb{R})$. By Lemmas 3.3, 3.4, $\widehat{J}_0$ is continuous on $\widetilde{E}$, then $\widehat{J}_0(v_n)\to\widehat{J}_0(\overline{v})$. Thus $\widehat{J}_0$ attains its minimum on S at a point $\overline{v}$ with $\|\overline{v}\|\le1$. It remains to prove that $\overline{v}\in S$.Indeed, using the relation $\varphi_v(s(v))=0$, we obtain for all $v\in S$ and $\xi\in[0,1]$ the following.

For convenience, set

$$A_\xi:=\int_{\mathbb{R}} e^{Q(t)}a(t)G(\xi v(t))\,dt, \tag{55}$$

$$B_\xi:=\int_{\mathbb{R}} e^{Q(t)}b(t)H(\xi v(t))\,dt. \tag{56}$$

Then

$$\begin{aligned} \frac{d}{d\xi}\widehat{J}_0(\xi v)&=\frac{d}{d\xi}\Big[\tfrac{1}{2}s^2(\xi v)+|s(\xi v)|^\nu A_\xi \\ &\qquad-|s(\xi v)|^\mu B_\xi\Big] \\ &=s(\xi v)s'(\xi v) \\ &\quad+\nu|s(\xi v)|^{\nu-2}s(\xi v)s'(\xi v)A_\xi \\ &\quad-\mu|s(\xi v)|^{\mu-2}s(\xi v)s'(\xi v)B_\xi \\ &\quad+\nu\frac{|s(\xi v)|^\nu}{\xi}A_\xi-\mu\frac{|s(\xi v)|^\mu}{\xi}B_\xi \\ &=s(\xi v)s'(\xi v)\Big[1+\nu|s(\xi v)|^{\nu-2}A_\xi \\ &\qquad-\mu|s(\xi v)|^{\mu-2}B_\xi\Big] \\ &\quad+\nu\frac{|s(\xi v)|^\nu}{\xi}A_\xi-\mu\frac{|s(\xi v)|^\mu}{\xi}B_\xi. \end{aligned} \tag{57}$$

By the defining relation $\varphi_v(s(v)) = 0$, the bracket vanishes, and we obtain Set $\sigma_\xi := s(\xi v)$. Then

$$\begin{aligned}\frac{d}{d\xi}\widehat{J}_0(\xi v) &= \frac{|\sigma_\xi|^2}{\xi}\Big[\nu|\sigma_\xi|^{\nu-2}A_\xi - \mu|\sigma_\xi|^{\mu-2}B_\xi\Big] \\ &= -\frac{|\sigma_\xi|^2}{\xi} < 0.\end{aligned} \tag{58}$$

Thus, $\widehat{J}_0(\xi v)$ decreases with respect to $\xi \in [0,1]$ and reaches its minimum at $\xi = 1$. This implies that $\widehat{J}_0$ attains its minimum on S at $\overline{v} \in S$. According to the spherical fibering method, we obtain that $\pm s(\overline{v})\overline{v}$ are two solutions of problem (1). ∎

Given that $\widehat{J}_0$ is an even function, bounded from below, weakly continuous, and of class C^1 on S, the Lusternik-Schnirelmann theory (as discussed in [**?**]) ensures that $\widehat{J}_0$ has a sequence of conditionally critical points $(v_n)_{n\in\mathbb{N}} \subset S$ such that $\widehat{J}_0(v_n) \to +\infty$ as $n \to \infty$. By applying Theorem 2.1, we deduce that when $h = 0$, the system (1) possesses a sequence of distinct solutions $(\pm u_n)_{n\in\mathbb{N}}$, where $u_n = s(v_n)v_n$ and $J_0(v_n) \to +\infty$ as $n \to \infty$.

4 Proof of Theorem 1.2

In the nonsymmetric case $h \neq 0$, the energy functional $J_h : E \to \mathbb{R}$ is defined by

$$\begin{aligned}J_h(u) &= \frac{1}{2}\int_{\mathbb{R}} e^{Q(t)}\big(|\dot{u}(t)|^2 + L(t)u(t)\cdot u(t)\big)\,dt \\ &\quad - \int_{\mathbb{R}} e^{Q(t)}W(t,u(t))\,dt \\ &= \frac{1}{2}\|u\|^2 + \int_{\mathbb{R}} e^{Q(t)}a(t)G(u(t))\,dt \\ &\quad - \int_{\mathbb{R}} e^{Q(t)}b(t)H(u(t))\,dt \\ &\quad - \int_{\mathbb{R}} e^{Q(t)}h(t)\cdot u(t)\,dt \\ &= J_0(u) - \int_{\mathbb{R}} e^{Q(t)}h(t)\cdot u(t)\,dt.\end{aligned} \tag{59}$$

For $u \in E$, we look for critical points of the form $u = sv,\ s \in \mathbb{R},\ v \in E,\ \|v\| = 1$.

Thus, extending J_h to $\mathbb{R}\times E$, we obtain

$$\begin{aligned}\widetilde{J}_h(s,v) &= \widetilde{J}_0(s,v) - s\int_{\mathbb{R}} e^{Q(t)}h(t)\cdot v(t)\,dt \\ &= \frac{s^2}{2}\|v\|^2 + |s|^\nu \int_{\mathbb{R}} e^{Q(t)}a(t)G(v(t))\,dt \\ &\quad - |s|^\mu \int_{\mathbb{R}} e^{Q(t)}b(t)H(v(t))\,dt \\ &\quad - s\int_{\mathbb{R}} e^{Q(t)}h(t)\cdot v(t)\,dt.\end{aligned} \tag{60}$$

for $(s,v) \in \mathbb{R}\times E$, and its restriction to $\mathbb{R}\times S$ is

$$\begin{aligned}\widetilde{J}_h(s,v) &= \frac{s^2}{2} + |s|^\nu \int_{\mathbb{R}} e^{Q(t)}a(t)G(v(t))\,dt \\ &\quad - |s|^\mu \int_{\mathbb{R}} e^{Q(t)}b(t)H(v(t))\,dt \\ &\quad - s\int_{\mathbb{R}} e^{Q(t)}h(t)\cdot v(t)\,dt.\end{aligned} \tag{61}$$

for $(s,v) \in \mathbb{R}\times S$. The bifurcation system $\frac{\partial \widetilde{J}_0}{\partial s}(s,v) = 0$ involves

$$\begin{aligned}&s + \nu|s|^{\nu-2}s\int_{\mathbb{R}} e^{Q(t)}a(t)G(v(t))\,dt \\ &\quad - \mu|s|^{\mu-2}s\int_{\mathbb{R}} e^{Q(t)}b(t)H(v(t))\,dt \\ &= \int_{\mathbb{R}} e^{Q(t)}h(t)\cdot v(t)\,dt.\end{aligned} \tag{62}$$

Let $\psi_v : \mathbb{R} \to \mathbb{R}$ be the function defined by

$$\begin{aligned}\psi_v(s) &= s + \nu|s|^{\nu-2}s\int_{\mathbb{R}} e^{Q(t)}a(t)G(v(t))\,dt \\ &\quad - \mu|s|^{\mu-2}s\int_{\mathbb{R}} e^{Q(t)}b(t)H(v(t))\,dt.\end{aligned} \tag{63}$$

Lemma 4.1. For every $v \in S$, the function ψ_v is odd, and it has a local minimum m_v and a local maximum M_v such that $M_v = -m_v$.

Proof : By derivation, we have

$$\begin{aligned}\psi_v'(s) &= 1 + \nu(\nu-1)|s|^{\nu-3}s\int_{\mathbb{R}} e^{Q(t)}a(t)G(v(t))\,dt \\ &\quad - \mu(\mu-1)|s|^{\mu-3}s\int_{\mathbb{R}} e^{Q(t)}b(t)H(v(t))\,dt.\end{aligned} \tag{64}$$

Since $1 < \nu < \mu$, we have $\lim_{s\to\infty}\psi_v'(s) = -\infty$ and

$$\lim_{s\to 0^+}\psi_v'(s) = \begin{cases} +\infty, & 1 < \nu < 2, \\ 1 + \nu(\nu-1)\displaystyle\int_{\mathbb{R}} e^{Q(t)}a(t)G(v(t))\,dt, & \nu = 2, \\ 1, & \nu > 2. \end{cases} \tag{65}$$

Thus ψ_v' has at least two zeros. Moreover,

$$\begin{aligned}\psi_v''(s) &= \nu(\nu-1)(\nu-2)|s|^{\nu-4}s\int_{\mathbb{R}} e^{Q(t)}a(t)G(v(t))\,dt \\ &\quad - \mu(\mu-1)(\mu-2)|s|^{\mu-4}s\int_{\mathbb{R}} e^{Q(t)}b(t)H(v(t))\,dt.\end{aligned} \tag{66}$$

If $1 < \nu \leq 2$, then $\psi_v''(s) < 0$ for $s > 0$. If $\nu > 2$, then

$$\bar{s}(v) = \left(\frac{\nu(\nu-1)(\nu-2)\int_{\mathbb{R}} e^{Q}aG(v)}{\mu(\mu-1)(\mu-2)\int_{\mathbb{R}} e^{Q}bH(v)}\right)^{1/(\mu-\nu)}. \tag{67}$$

Hence ψ_v' has exactly two zeros $\pm s(v)$. As in Lemma 3.4, $s(v)$ is C^1 on $\widetilde{E}$.

Since $\lim_{s\to\infty}\psi_v'(s)=-\infty$ and ψ_v is odd, it admits a local minimum m_v and a local maximum M_v with $M_v=-m_v$. ∎

Lemma 4.2.
If $\|h\|_{L_Q^{\mu'}} < (\mu-2)\Big[\mu(\mu-1)^{\mu-1}\eta_\mu^{2(\mu-1)}M_bM_H\Big]^{-\frac{1}{\mu-2}}$, where μ' is the conjugate exponent of μ, then equation

$$\psi_v(s)=\int_{\mathbb{R}} e^{Q(t)}h(t)\cdot v(t)\,dt. \tag{68}$$

has three distinct solutions.

Proof: Set

$$\overline{\psi}_v(s)=s-\mu|s|^{\mu-2}s\int_{\mathbb{R}} e^{Q(t)}b(t)H(v(t))\,dt. \tag{69}$$

We have $\psi_v\geq\overline{\psi}_v$ and, denoting by $\overline{M}_v$ the local maximum of $\overline{\psi}_v$,

$$\begin{aligned}\overline{M}_v&=\overline{\psi}_v\Big(\big[\mu(\mu-1)\int_{\mathbb{R}}e^{Q}bH(v)\,dt\big]^{-\frac{1}{\mu-2}}\Big)\\&=(\mu-2)\Big[\mu(\mu-1)^{\mu-1}\int_{\mathbb{R}}e^{Q}bH(v)\,dt\Big]^{-\frac{1}{\mu-2}}.\end{aligned} \tag{70}$$

Hölder's inequality implies

$$\begin{aligned}&\Big|\int_{\mathbb{R}}e^{Q(t)}h(t)\cdot v(t)\,dt\Big|\Big(\int_{\mathbb{R}}e^{Q}bH(v)\,dt\Big)^{\frac{1}{\mu-2}}\\&\leq\|h\|_{L_Q^{\mu'}}\|v\|_{L_Q^{\mu}}\big(M_bM_H\|v\|_{L_Q^{\mu}}^{\mu}\big)^{\frac{1}{\mu-2}}\\&\leq\|h\|_{L_Q^{\mu'}}\big(M_bM_H\eta_\mu^{2(\mu-1)}\big)^{\frac{1}{\mu-2}}.\end{aligned} \tag{71}$$

If we take

$$\|h\|_{L_Q^{\mu'}}<(\mu-2)\Big[\mu(\mu-1)^{\mu-1}\eta_\mu^{2(\mu-1)}M_bM_H\Big]^{-\frac{1}{\mu-2}}. \tag{72}$$

, then Hölder's inequality implies

$$\begin{aligned}&\sup_{v\in S}\Bigg[\Big|\int_{\mathbb{R}}e^{Q(t)}h(t)\cdot v(t)\,dt\Big|\\&\quad\times\Big(\int_{\mathbb{R}}e^{Q(t)}b(t)H(v(t))\,dt\Big)^{\frac{1}{\mu-2}}\Bigg]\\&\quad<(\mu-2)\big[\mu(\mu-1)^{\mu-1}\big]^{\frac{1}{\mu-2}}.\end{aligned} \tag{73}$$

Since $M_v\geq\overline{M}_v$, then (70), (73) imply

$$\Big|\int_{\mathbb{R}}e^{Q(t)}h(t)\cdot v(t)dt\Big|<\overline{M}_v\leq M_v$$

which implies that system (62) has three distinct solutions. ∎

Given the bifurcation system (62) with three distinct solutions $s_i(v)$, $i=1,2,3$, we consider the three induced functionals

$$\begin{aligned}\widehat{J}_{h,i}(v)&=\frac{1}{2}|s_i(v)|^2+|s_i(v)|^{\nu}\int_{\mathbb{R}}e^{Q(t)}a(t)G(v(t))\,dt\\&\quad-|s_i(v)|^{\mu}\int_{\mathbb{R}}e^{Q(t)}b(t)H(v(t))\,dt\\&\quad-s_i(v)\int_{\mathbb{R}}e^{Q(t)}h(t)\cdot v(t)\,dt.\end{aligned} \tag{74}$$

which are defined and distinct on $B\setminus\{0\}$, where $B=\{v\in E/\|v\|\leq 1\}$. Using Hölder's inequality and the properties of the bifurcation system (62), we obtain

$$\begin{aligned}\widehat{J}_{h,i}(v)&=\widehat{J}_{0,i}(v)-s_i(v)\int_{\mathbb{R}}e^{Q(t)}h(t)\cdot v(t)\,dt\\&\geq\Big(\tfrac{1}{2}-\tfrac{1}{\mu}\Big)s_i(v)^2\\&\quad+\Big(1-\tfrac{\nu}{\mu}\Big)|s_i(v)|^{\nu}\int_{\mathbb{R}}e^{Q(t)}a(t)G(v(t))\,dt\\&\quad+\Big(\tfrac{1}{\mu}-1\Big)\eta_\mu\|h\|_{L_Q^{\mu'}}|s_i(v)|.\end{aligned} \tag{75}$$

Since $\max\{2,\nu\}<\mu$, it follows that $\widehat{J}_{h,i}$ is bounded from below. By applying Lemmas 3.3 and 3.4, we know that $\widehat{J}_{h,i}$ is continuously differentiable on the space $\widetilde{E}=L_Q^2(\mathbb{R})\cap L_Q^{\mu}(\mathbb{R})$. Combining this with Lemma 2.1, we conclude that $\widehat{J}_{h,i}$ is weakly continuous on the space E. Therefore, $\widehat{J}_{h,i}$ attains its minimum on the set S at some point $\overline{v}_i\in B$ where $s_i(\overline{v}_i)\neq 0$. What remains to be shown is that $\overline{v}_i\in S$. Indeed, by utilizing equation (62), we can demonstrate for any $v\in S$ and $\xi\in[0,1]$ that

$$\begin{aligned}\frac{d}{d\xi}(\widehat{J}_{h,i}(\xi v))&=\frac{d}{d\xi}\Big[\tfrac{1}{2}s_i(\xi v)^2+|s_i(\xi v)|^{\nu}A_\xi\\&\qquad-|s_i(\xi v)|^{\mu}B_\xi-s_i(\xi v)H_\xi\Big]\\&=s_i'(\xi v)\Big[s_i(\xi v)+\nu|s_i(\xi v)|^{\nu-2}s_i(\xi v)A_\xi\\&\qquad-\mu|s_i(\xi v)|^{\mu-2}s_i(\xi v)B_\xi-H_\xi\Big]\\&\quad+\frac{\nu}{\xi}|s_i(\xi v)|^{\nu}A_\xi-\frac{\mu}{\xi}|s_i(\xi v)|^{\mu}B_\xi\\&\quad-s_i(\xi v)\int_{\mathbb{R}}e^{Q(t)}h(t)\cdot v(t)\,dt\\&=\frac{s_i(\xi v)}{\xi}\Big[\nu|s_i(\xi v)|^{\nu-2}s_i(\xi v)A_\xi\\&\qquad-\mu|s_i(\xi v)|^{\mu-2}s_i(\xi v)B_\xi-H_\xi\Big]\\&=-\frac{|s_i(\xi v)|^2}{\xi}<0,\end{aligned} \tag{76}$$

where

$$A_\xi := \int_{\mathbb{R}} e^{Q(t)} a(t) G(\xi v(t))\, dt,$$
$$B_\xi := \int_{\mathbb{R}} e^{Q(t)} b(t) H(\xi v(t))\, dt, \tag{77}$$
$$H_\xi := \int_{\mathbb{R}} e^{Q(t)} h(t) \cdot \xi v(t)\, dt.$$

As ξ varies over $[0,1]$, $\widehat{J}_{h,i}(\xi v)$ decreases, reaching its minimum when $\xi = 1$. This minimum occurs at $\overline{v}_i \in S$, indicating that $\widehat{J}_{h,i}$ achieves its minimum on S at $\overline{v}_i$. According to the spherical fibering method, the solutions $\pm s_i(\overline{v}_i)\overline{v}$ represent three solutions of problem (1).

References

1. M. Izydorek and J. Janczewska, Homoclinic solutions for a class of the second order Hamiltonian systems, J. Differential Equations 219(2), 375–389 (2005). DOI: https://doi.org/10.1016/j.jde.2005.06.029
2. J. Jiang, S. Lu, X. Lv, Homoclinic solutions for a class of second order Hamiltonian systems, Nonlinear Analysis: Real World Applications 13, 176–185 (2012). DOI: https://doi.org/10.1016/j.nonrwa.2011.07.016
3. S. Lu, X. Lv and P. Yan, Existence of homoclinics for a class of Hamiltonian systems, Nonlinear Analysis 72, 390–398 (2010). DOI: https://doi.org/10.1016/j.na.2009.06.073
4. P.H. Rabinowitz, Homoclinic orbits for a class of Hamiltonian systems, Proc. Roy. Soc. Edinburgh 114A, 33–38 (1990). DOI: https://doi.org/10.1017/S0308210500024240
5. X.H. Tang, L. Xiao, Homoclinic solutions for a class of second order Hamiltonian systems, Nonlinear Analysis 71, 1140–1152 (2009). DOI: https://doi.org/10.1016/j.na.2008.11.039
6. R. Yuan, Z. Zhang, Homoclinic solutions for some second order nonautonomous Hamiltonian systems without the globally superquadratic condition, Nonlinear Analysis 72, 1809–1819 (2010). DOI: https://doi.org/10.1016/j.na.2009.09.011
7. G. Chen, Homoclinic orbits for second order Hamiltonian systems with asymptotically linear terms at infinity, Advances in Difference Equations 2014(114), (2014). DOI: https://doi.org/10.1186/1687-1847-2014-114
8. G. Chen, Z. He, Infinitely many homoclinic solutions for a class of second order Hamiltonian systems, Advances in Difference Equations 2014(161), (2014). DOI: https://doi.org/10.1186/1687-1847-2014-161
9. L. Chu, Q. Zhang, Homoclinic solutions for a class of second order Hamiltonian systems with locally defined potentials, Nonlinear Analysis 75, 3188–3197 (2012). DOI: https://doi.org/10.1016/j.na.2011.12.015
10. Y. Ding, Existence and multiplicity results for homoclinic solutions to a class of Hamiltonian systems, Nonlinear Analysis 25(11), 1095–1113 (1995). DOI: https://doi.org/10.1016/0362-546X(94)00156-Q
11. X. Lin and X.H. Tang, Homoclinic solutions for a class of second order Hamiltonian systems, J. Math. Anal. Appl. 354, 539–549 (2009). DOI: https://doi.org/10.1016/j.jmaa.2008.12.048
12. X. Lin and X.H. Tang, Infinitely many homoclinic orbits for Hamiltonian systems with indefinite sign subquadratic potentials, Nonlinear Analysis 74, 6314–6325 (2011). DOI: https://doi.org/10.1016/j.na.2011.06.038
13. C. Liu, Q. Zhang, Infinitely many homoclinic solutions for second order Hamiltonian systems, Nonlinear Analysis 72, 894–903 (2010). DOI: https://doi.org/10.1016/j.na.2009.07.016
14. P.H. Rabinowitz and K. Tanaka, Some results on connecting orbits for a class of Hamiltonian systems, Math. Z. 206(3), 473–499 (1991). DOI: https://doi.org/10.1007/BF02571368
15. J. Sun, T-f. Wu, Homoclinic solutions for a second order Hamiltonian system with a positive semi-definite matrix, Chaos, Solitons and Fractals 76, 24–31 (2015). DOI: https://doi.org/10.1016/j.chaos.2015.04.006
16. J. Sun, T-f. Wu, Multiplicity and concentration of homoclinic solutions for some second order Hamiltonian systems, Nonlinear Analysis 114, 105–115 (2015). DOI: https://doi.org/10.1016/j.na.2014.11.007
17. C.L. Tang, Li-Li Wan, Existence of homoclinic orbits for second order Hamiltonian systems without (AR) condition, Nonlinear Analysis 74, 5303–5313 (2011). DOI: https://doi.org/10.1016/j.na.2011.04.067
18. J. Wei, J. Wang, Infinitely many homoclinic orbits for the second order Hamiltonian systems with general potentials, J. Math. Anal. Appl. 366(2), 694–699 (2010). DOI: https://doi.org/10.1016/j.jmaa.2010.01.038
19. Z. Zhang, Existence of homoclinic solutions for second order Hamiltonian systems with general potentials, J. Appl. Math. Comput. 44, 263–272 (2014). DOI: https://doi.org/10.1007/s12190-013-0694-6
20. R.P. Agarwal, P. Chen and X. Tang, Fast homoclinic solutions for a class of damped vibration problems, Applied Mathematics and Computation 219, 6053–6065

(2013). DOI: https://doi.org/10.1016/j.amc.2012.12.005

21. P. Chen and X.H. Tang, Fast homoclinic solutions for a class of damped vibration problems with sub-quadratic potentials, Math. Nachr. 286(1), 4–16 (2013). DOI: https://doi.org/10.1002/mana.201100258
22. F. Khelifi, M. Timoumi, Even homoclinic orbits for a class of damped vibration systems, Indagationes Mathematicae 28(6), 1111–1125 (2017). DOI: https://doi.org/10.1016/j.indag.2017.08.001
23. M. Timoumi, Infinitely many fast homoclinic solutions for a class of superquadratic damped vibration systems, Journal of Elliptic and Parabolic Equations 6, 451–471 (2020). DOI: https://doi.org/10.1007/s41808-020-00071-3
24. M. Timoumi, On ground state homoclinic orbits of a class of superquadratic damped vibration systems, Mediterr. J. Math. 15, Article 214 (2018). DOI: https://doi.org/10.1007/s00009-018-1212-8
25. R. Yuan and Z. Zhang, Fast homoclinic solutions for some second order non-autonomous systems, J. Math. Anal. Appl. 376, 51–63 (2011). DOI: https://doi.org/10.1016/j.jmaa.2010.10.045

TTMP vol 3 (1), 2026
doi: 10.30511/TTMP.2026.2086335.1072

Transactions in Theoretical and Mathematical Physics

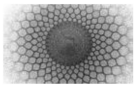

Lie Algebraic Approaches to Advanced Few-Body Hamiltonians in Physics

H. Rahmati[a,1]

[1]Department of Physics, Qom University of Technology,
Qom 37195-1519, Iran

Received: 22 January 2026 / Accepted: 22 February 2026 / Published: 23 February 2026

Abstract In quantum many-body systems, the emergence of complex interactions generally prevents the straightforward application of conventional analytical methods such as direct solution of the Schrödinger equation, variation theory, or the WKB approximation. An alternative algebraic perspective, employing techniques such as representation theory, reduction transformations, and gauge transformations, provide successful ways by identifying the hidden Lie algebra underlying a given problem.
On the other hand, few-body systems remain challenging, as their symmetries are limited rather than N-body cases. In this work, we demonstrate that by incorporating geometric insight, one may establishes a meaningful connection between the mathematical structure and the physical content of the problem.

Keywords. Lie algebraic approach, geometry, two-body and three-body problem, Hellmann potential

1 Introduction

Since the early twentieth century and the development of quantum mechanics, it became clear that new mathematical frameworks were required. The use of Lie algebra representations in solving problems such as the simple harmonic oscillator and the hydrogen atom constituted early successful efforts in this direction [1]. Beginning around 1970, mathematical physicists such as Calogero, Perelomov, and others systematically applied Lie algebraic methods to the study of quantum N-body systems [2, 3]. In such systems, symmetry simplifies many relations and often leads to closed-form expressions for wave functions and eigenvalues.
Group theory allows classification of the possible quantum states of a system purely on the basis of its symmetries (e.g., rotational, translational, and permutation symmetry), and even enables prediction of system behavior prior to explicitly solving the Schrödinger equation or experiencing the true results in the lab. A familiar example is the hydrogen atom. Its symmetry is described by the group $SO(4)$, which extends beyond the ordinary spherical symmetry $SO(3)$ [4]. The Radial part of the Hydrogen atom in terms of Schrodinger equation simplifies to

$$-\frac{1}{\rho^2}\frac{d}{d\rho}(\rho^2\frac{dR(\rho)}{d\rho})+[-\frac{l(l+1)}{\rho^2}+\frac{2}{\rho}-\varepsilon]R(\rho)=0 \qquad (1)$$

Moreover, using the rotational symmetry and invariance of the Runge–Lenz vector in the hydrogen atom,

$$M^2=\frac{1}{4}(-1-\frac{\mu}{2H(n,l)}) \qquad (2)$$

One can directly obtain the energy eigenvalues by acting on the wave function

$$\varepsilon=-\frac{\mu}{2n^2} \qquad (3)$$

However, in few-body systems, the structure of the systems have limited geometrical symmetries respect to the N-body cases. In fact, infinite representations of the symmetry in the systems in few-body problems, changes to the specified geometric structures governing the system [5, 6]. By introducing a geometric perspective, one can take an effective step toward solving the problem. In this work, we employ this geometric interpretation to analyze two few-body physical problems and obtain their energy spectra.

2 From Differential Equations to Hidden Algebraic Structure: A Historical Perspective

A manifest symmetry is a transformation readily visible in the geometry of the system, such as the rotational symmetric

[a]e-mail: hrahmati1357@yahoo.com

operators in a sphere. A hidden symmetry, by contrast, is not apparent in configuration space but is encoded in the governing equations (e.g., the Schrödinger equation) and profoundly controls physical properties such as the energy spectrum.

The identification of hidden symmetry proceeds through the following steps:

1. For a given Hamiltonian H, identify a set of operators O_i: $[H, O_i] = 0$
2. Verify closure of the algebra generated by these operators $[O_i, O_j] = \imath\hbar f_{ij}^k O_k$
3. Compare the resulting algebraic relations with known Lie algebras $gl(n,R)$, $sl(n,R)$, $so(n)$, $su(n)$, ... to reveal the underlying algebra of the problem.

Following the introduction of quantum N-body models by Calogero and Sutherland, these systems became a fertile area of research in both mathematics and physics [7]. In these models, particles are arranged on a symmetric lattice and interact through inverse-square rational or trigonometric potentials

$$H_{Cal} = \frac{1}{2}\sum_{i=1}^{N}(-\frac{d^2}{dx_i^2} + \omega^2 x_i^2) + g\sum_{1\le i<j\le N}^{N}\frac{1}{(x_i - x_j)^2}$$
$$H_{Sut} = \frac{1}{2}\sum_{i=1}^{N} -\frac{d^2}{dx_i^2} + g\sum_{1\le i<j\le N}^{N}\frac{1}{\sin^2(x_i - x_j)} \tag{4}$$

Calogero introduced Dunkl operators

$$D_i = \frac{\partial}{\partial x_i} + \beta\sum_{i\neq j}^{N}\frac{1}{x_i - x_j}(1 - K_{ij}) \tag{5}$$

and demonstrated that their commutation relations provide a sufficient condition for integrability and solvability

$$[D_i, D_j] = 0 \tag{6}$$

One of the pioneering algebraic approaches to the Calogero and Sutherland models was developed by Olshanetsky and Perelomov [8]. In this framework, the Hamiltonian is formulated in terms of the root system of a semi simple Lie algebra as a differential equation

$$H = \frac{1}{2}\sum_{i=1}^{N} P_i^2 + \sum_{\alpha\in\phi^+}\frac{g}{(\alpha.x)^2}, \quad g = \beta(\beta - 1) \tag{7}$$

For example, the rational Calogero model corresponds to a_n Lie algebra root system

$$\phi^+ = e_i - e_j, \quad i < j \tag{8}$$

While the Sutherland Hamiltonian represents its trigonometric version. The wave function is likewise determined by the root structure too:

$$\psi_0(x) = \prod_{\alpha\in\phi^+}(\alpha.x)^2 \tag{9}$$

In this sense, the hidden algebra of both models is the same, and the two potentials represent two aspects of a single algebraic structure. The essential idea is to relate symmetric spaces to quantum systems through representation theory, such that the Hamiltonian assumes the form of a Laplace Beltrami operator on the associated symmetric space.

In Turbiner's approach, one starts from the Hamiltonian derived from the root system and selects a polynomial space invariant under the Hamiltonian. For the Calogero Hamiltonian, such a space can be constructed explicitly

$$a_n : V_n = \{x, x^2, x^3, \ldots, x^n\} \tag{10}$$

One then identifies differential operators that act as generators of a Lie algebra (e.g., gl_n or sl_n) preserving this space by the algebraic generators

$$J_i^- = \frac{\partial}{\partial x_i}, \quad J_{i,j}^0 = x_i J_j^-,$$
$$J_0 = n - \sum_{i=1}^{N} x_p\frac{\partial}{\partial x_p}, \quad J_i^+ = x_i J_0 \tag{11}$$

The Hamiltonian can then be rewritten as a second-degree polynomial in these generators and solved accordingly. In such systems, solvability arises from the existence of a hidden algebraic structure revealed through reduction [9].

Kamran's method begins from a fully mathematical standpoint, constructing the most general differential equation L_i based on first-order Lie algebra generators. By identifying an appropriate mapping, one establishes equivalence between the general quasi-exactly solvable operator

$$T = \sum_{i,j=1}^{N} C_{ij}L_iL_j + \sum_{i=1}^{N} C_iL_i + C_0 \tag{12}$$

and the Schrödinger equation. A central theorem in this case states that if a second-order differential operator satisfies certain structural conditions, based on Bochner's theorem, then through a suitable change of variables and gauge transformations, it can be cast into Schrödinger form with a well-defined potential [10, 11].

3 Few-Body Systems and Two Applications of the Algebraic–Geometric Approach

Many-body systems in nature are composed of interacting few-body subsystems. To understand thermodynamic, optical, and chemical properties of composite materials, one often first precisely characterize the quantum properties of their few-body building blocks. Quantum phenomena such as entanglement are more transparently observable in few-body systems. Although these effects persist in many-body systems, collective interactions complicate their control and

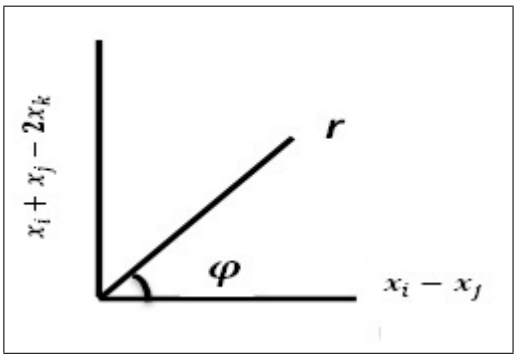

Fig. 1 Jacobi coordinates

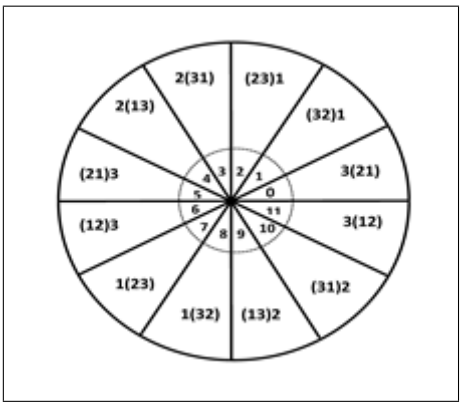

Fig. 2 D_{12} Lie group

analysis. Moreover, the development of quantum technologies such as quantum computing requires a detailed understanding of few-body systems [12].
For example, the exact solution of the Calogero Hamiltonian is expressed in terms of Jack polynomials

$$J_\lambda^\alpha(x_1,x_2,\ldots,x_N) = \sum_{\mu\le\lambda} c_{\mu\lambda}(\alpha) m_\mu(x_1,x_2,\ldots,x_N)$$
$$m_\mu(x_1,x_2,\ldots,x_N) = \sum x_1^{\lambda_1} x_2^{\lambda_2}\ldots x_N^{\lambda_N} \tag{13}$$

These polynomials are constructed from monomials m_μ corresponding to partitions of the system $\lambda = (\lambda_1,\lambda_2,\ldots,\lambda_N)$ by the condition $\lambda_1 \ge \lambda_2 \ge \ldots \ge \lambda_N$. For large particle numbers, writing these polynomials explicitly becomes highly nontrivial [13].
Another challenge arises in atoms with some valence electrons. Accounting for their interaction with lower-energy orbitals typically requires extensive computations not easily handled by conventional methods. We now examine two few-body problems within this algebraic–geometric framework.

3.1 A Three-Body Problem with Sutherland-Type Potential

Firstly, we consider a system of three distinguishable fermions interacting through two-body and three-body Sutherland-type potentials as follows [14]

$$H = \frac{1}{2}\sum_{i=1}^{3} -\frac{d^2}{dx_i^2} + g_\nu \sum_{1\le i\ne j\le 3} \frac{1}{\sin^2(x_i - x_j)} + g_\mu \sum_{1\le i\ne j\ne k\le 3} \frac{1}{\sin^2(x_i + x_j - 2x_k)} \tag{14}$$

By introducing Jacobi coordinates, Fig.1, the center-of-mass motion is separated from relative motion, revealing translational symmetry and reducing the number of variables

$$x_i - x_j = r\cos\phi, \quad x_i + x_j - 2x_k = r\sin\phi \tag{15}$$

The equation of motion separates into radial and angular parts

$$(-\frac{\partial^2}{\partial r^2} - \frac{1}{r}\frac{\partial}{\partial r} + \frac{\lambda^2}{r^2} - E)R(r) = 0$$
$$(-\frac{\partial^2}{\partial \phi^2} + \frac{9g_\nu}{\sin^2 3\phi} + \frac{9g_\mu}{\cos^2 3\phi} - \lambda^2)\Phi(\phi) = 0 \tag{16}$$

Consistency of the angular equation imposes a condition $\cos 6\phi \ne \pm 1$ leading to twelve admissible angular states, producing an elegant discrete symmetry in the problem. Due to the discrete symmetry associated with the Lie algebra D_{12}, Fig.2, in the reduced geometric space, the quantum calculations simplify considerably. Solving the Schrödinger equation in only one region of twelve configuration spaces suffices to determine all physical properties. Performing a reduction transformation and appropriate change of variables $z_j = \exp(2\imath a(R - x_{kl}))$, where $x_{kl} = x_k - x_l$ and $R = \frac{x_1+x_2+x_3}{3}$ the Hamiltonian separates into a center-of-mass term and a differential operator corresponding to a three-variable Jack polynomial structure

$$\tilde{H} = 6\frac{\hbar^2 a^2}{m}[\sum_{j=1}^{3}(z_j\frac{\partial}{\partial z_j})^2 + (\nu+\mu)\sum_{j.k=1,j\ne k}^{3}\frac{z_j+z_k}{z_j-z_k}(z_j\frac{\partial}{\partial z_j})] + \frac{4}{3}\frac{\hbar^2 a^2}{m}(\sum_{j=1}^{3} z_j\frac{\partial}{\partial z_j}))^2 \tag{17}$$

The resulting energy spectrum for the three distinguishable fermions is obtained in closed form

$$E_{rel} - E_0 = 4(\nu^2 - 3\mu^2 + 6(\nu+\mu) + 3) \tag{18}$$

3.2 B Screening in Alkali Atoms and the Hellmann Potential

Perturbation theory plays a central role in quantum mechanics; we apply Lie algebraic symmetry methods derived from

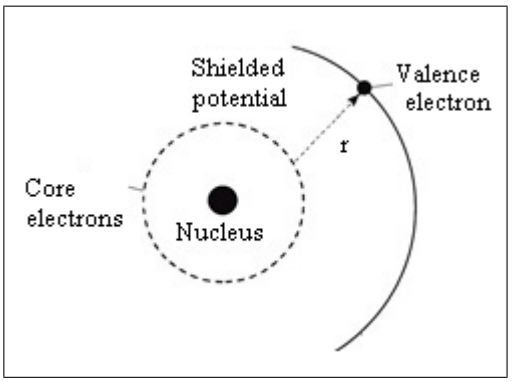

Fig. 3 Screening effect

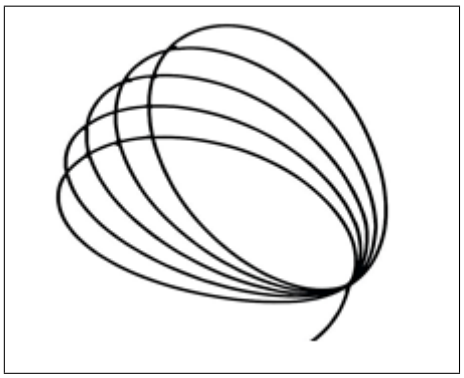

Fig. 4 Precession motion in the Hellmann potential

the hydrogen atom to the Hellmann potential, which is of Yukawa type added to Coulomb potential [15]

$$V(r) = -\frac{1}{r} + \frac{-Z}{r}\Upsilon e^{-\frac{\delta r}{Z}}, \quad \Upsilon = \frac{Z-1}{Z} \tag{19}$$

This potential arises naturally in alkali atoms, where inner electrons screen the nuclear charge experienced by the outermost electron, leading to deviations from the Coulomb potential and affecting the energy levels, Fig.3. The method proceeds by relating the perturbative term to the precessional motion of the Runge–Lenz vector

$$\overrightarrow{M} = \frac{1}{2\mu}(\overrightarrow{P} \times \overrightarrow{L} - \overrightarrow{L} \times \overrightarrow{P}) - \frac{Z}{r^2}\overrightarrow{r} \tag{20}$$

Whose Lie algebra $SO(4)$ is

$$so(4) = so(3) \bigoplus so(3) \tag{21}$$

And its Lie algebraic commutation relations are

$$\begin{aligned} &[L_i, L_j] = \imath\varepsilon_{ijk}L_k, \quad [L_i, M_j] = \imath\varepsilon_{ijk}M_k, \\ &[M_i, M_j] = \imath\varepsilon_{ijk}(-2\frac{E(n,l)}{\mu})L_k \end{aligned} \tag{22}$$

In the Hellmann potential, the Runge–Lenz vector undergoes precession, and the orbital ellipse is no longer closed, Fig.4. The perturbation effectively renders the algebra non-connected, which underlies the non-solvability of the system.

The perturbation could be corresponded as the Yukawa component of the Hellmann potential

$$p(r) = -\frac{Z-1}{r}\Upsilon)e^{-\frac{\delta r}{Z}} \tag{23}$$

The operator describing precession over one period T is

$$\Omega = \frac{\partial}{\partial L}(\frac{1}{T}\int p(r)dt) \tag{24}$$

We demonstrate that within the convergence domain determined by Cauchy estimates, stable energy eigenvalues can be obtained

$$|\frac{e^{-\frac{\delta r}{Z}}}{r}|_{R-\delta} \leq |\frac{-Z}{\delta r^2}|_R \tag{25}$$

Applying Kolmogorov's theorem [16]

$$p(r) \to O(-\frac{Z}{\delta r^2}^2) \tag{26}$$

Rewriting the Runge–Lenz vector operator within this approximation yields the corrected Hellmann potential spectrum.
Comparison with alternative computational methods shows good agreement for low-lying energy levels, Table 1, although discrepancies increase for higher levels due to more intricate interactions.

4 Conclusion and Discussion

Since 1969, significant progress has been made in solving many-body problems using Lie algebraic techniques. However, some of these methods are not fully effective for few-body systems. For example, specified symmetries exists for constructing wave functions of three- or four-body systems from the general N-body formalism, having more access to general symmetries and bigger geometric viewpoint.
From a practical standpoint, atoms with a finite number of interacting electrons present complex challenges in determining wave functions and energy spectra. In this work, by solving two such problems, we have shown that incorporating a geometric interpretation not only clarifies the physical meaning but also simplifies the solution procedure.
Nonetheless, this method has some limitations. Real physical systems frequently involve external fields, thermal effects, and explicit symmetry breaking. This demand could be answered

Table 1 comparison of our results and other methods

state	δ	our results	NU [17]	Ref [18]
$2P$	0.01	-0.07396007816	-0.077500	-0.072020
$3P$	0.01	-0.03297991942	-0.029279	-0.036644
$3d$	0.01	-0.04226536099	-0.043825	-0.036813
$4P$	0.01	-0.02561419824	-0.030925	-0.023641
$4d$	0.01	-0.04061691390	-0.031356	-0.023841
$4f$	0.01	-0.01894820393	-0.032356	-0.024056

1. The role of Lie algebra and group theory is to provide a precise structural understanding of the mathematical symmetries, while the ultimate solution of the physical problem depends on the specific dynamics;
2. According to Noether's theorem, symmetries are directly associated with conserved quantities. By first analyzing the ideal symmetric system and identifying its conserved quantities, one can then systematically investigate the geometric or algebraic mechanisms that break these symmetries. Thereby a more comprehensive understanding than a purely phenomenological approach would be provided.

5 Acknowledgements

The manuscript was written by the author and AI tools were used only for language editing and translation.

References

1. J. J. Sakurai, *Modern Quantum Mechanics*, (Addison-Wesley, 1985)
2. F. Calogero, Solution of the one-dimensional N-body problems Problems with Quadratic and/or Inversely Quadratic Pair Potentials, J. Math. Phys. **12**, 419 (1971). DOI: https://doi.org/10.1063/1.1665604
3. B. Sutherland, Exact Results for a Quantum Many-Body Problem in One Dimension, Phys. Rev. A **5**, 1372 (1972). DOI: https://doi.org/10.1103/PhysRevA.5.1372
4. R. Gilmore, *Lie Groups, Physics and Geometry*, (Cambridge University Press, 2008)
5. F. Pan and J. P. Draayer, Exact Solutions for Some Nuclear Many-Body Problems, Ann. Phys. **271**, 120 (1999). DOI: https://doi.org/10.1006/aphy.1998.5870
6. J. F. Cariñena, J. de Lucas, A. Ramos, A geometric approach to time evolution operators of Lie quantum systems, Int. J. Theor. Phys. **48**, 1379 (2009). DOI: https://doi.org/10.1007/s10773-009-9911-0
7. F. Calogero, *Classical Many Body Problems Amenable to Exact Treatments in One, Two and Three Dimensional Space*, (Springer-Verlag Berlin Heidelberg, 2001)
8. M. A. Olshanetsky and A. M. Perelomov, Quantum Integrable Systems Related to Lie Algebras, Phys. Rep. **94**, 313 (1983). DOI: https://doi.org/10.1016/0370-1573(83)90018-2
9. A. V. Turbiner, Quasi Exactly Solvable Problems and $SL(2)$ Algebra, Commun. Math. Phys. **118**, 467 (1988). DOI: https://doi.org/10.1007/BF01466727
10. A. G. López, N. Kamran and P. J. Olver, New Quasi Exactly Solvable Hamiltonians in Two Dimensions, Commun. Math. Phys. **159**, 503 (1994). DOI: https://doi.org/10.1007/BF02100490
11. D. Gómez-Ullate, N. Kamran, R. Milson, An Extension of Bochner's problem: Exceptional Invariant Subspaces, J. Approx. Theory **162**, 987 (2010). DOI: https://doi.org/10.1016/j.jat.2009.11.002
12. F. Brauneis et al., Comparison of renormalized interactions using one-dimensional few-body systems as a testbed, Phys. Rev. A **111**, 013303 (2025). DOI: https://doi.org/10.1103/PhysRevA.111.013303
13. I. G. Macdonald, *Symmetric Functions and Hall Polynomials, 2nd edition*, (Clarendon Press, Oxford, 1995)
14. H. Rahmati, A. Latifi, Exact solution of the two and three-body interactions in the trigonometric three-body problem via Jack polynomials, Few-Body Syst. **60**, 1 (2019). DOI: https://doi.org/10.1007/s00601-019-1464-5
15. H. Rahmati, Lie algebraic approach to the Hellmann Hamiltonian by considering perturbation method, Theor. Math. Phys. **221**, 2144 (2024). DOI: https://doi.org/10.1134/S0040577924120121
16. A. N. Kolmogorov, On conservation of conditionally periodic motions for a small change in Hamilton's function, Dokl. Akad. Nauk SSSR **98**, 527 (1954)
17. M. Hamzavi, K. E. Thylwe, and A. A. Rajabi, Approximate bound states solution of the Hellmann potential, Commun. Theor. Phys. **60**, 1 (2013). DOI: https://doi.org/10.1088/0253-6102/60/1/01
18. S. M. Ikhdair and R. Sever, A perturbative treatment for the bound states of the Hellmann potential, J. Mol. Struct. **809**, 103 (2007). DOI: https://doi.org/10.1016/j.molstruc.2006.06.028

TTMP vol 3 (1), 2026
doi: 10.30511/TTMP.2026.2083409.1070

Transactions in Theoretical and Mathematical Physics

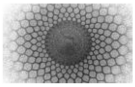

A Dynamical Physics Equation for Cell Proliferation

Javad Sharifi[a]

[1]Electrical and Computer Engineering Department, Qom University of Technology

Received: 07 January 2026 / Accepted: 20 February 2026 / Published: 23 February 2026

Abstract. A dynamical model for mitosis cell proliferation from a geometric viewpoint is derived. The derived kinetics are nonlinear partial differential equations of cell volume and mass density. We consider the process of inherent cell growth due to biological processes as the mass increase in the cell which exerts force inside of the cell. Likewise, the process of segregation is viewed as a mass decrease. We consider the physical aspects of inherent biological processes such as anabolism of structural proteins and lipids swelling due to mass influx and shrinking due to mass outflow. To this aim, by first and second equations of motion together with Fick's laws of diffusion for nutrition, we model this force and obtain the cell radius function and mass density evolution equations. The control action will appear in our dynamic equation.

Keywords: Dynamic Physics Equation; Cell Proliferation; Fick Laws

1 Introduction

We can model biological processes and bio-systems with the aim of physical laws and system insight. Furthermore, by control theory of biological and biophysical processes, a new field of sciences such as system biology, system biophysics, etc., has been created. This system's viewpoints opened new windows to physics and life science. From the biophysical and biological control side, it makes it possible to study many biological processes such as gene regulatory networks (GRN) [1–5], genetic switch [6, 7], and DNA computing [8–12], which is suited for technology developments.

Someone may view cell proliferation systematically to infer new sophisticated medical methods for stem cell differentiation technology, cancer cure, etc. The well-known cell cycle entails an ordered series of macromolecular events that lead to cell division and the production of two daughter cells, each containing chromosomes identical to those of the parental cell [13]. A brief illustration of cell mitosis is depicted in Fig. 1. In normal cells, several genes control the process of cell division. Normal growth requires a balance between the activity of genes, those that promote cell proliferation, and those that suppress it. It also relies on the activities of genes that signal when damaged cells should undergo apoptosis. Cells become cancerous after mutations accumulate in the various genes that control cell proliferation. Deregulated cell proliferation led to cancer and many diseases [14].

From a physical and geometrical viewpoint, cancer cells divide more rapidly than their progenitors and become less dependent on signals from other cells. Cancer cells even evade programmed cell death, even though their multiple abnormalities would normally make them prime targets for apoptosis. In the late stages of cancer, cells break through normal tissue boundaries and metastasize to new sites in the body. In other words, cancer can occur when cell division rates accelerate or by inhibition of normal controls on the cell cycle arrest or programmed cell death. From a control system viewpoint, cancer cell dynamics are different from normal cell dynamics. Hence, by dynamic modeling of normal cell proliferation and then by designing an appropriate control strategy it would be possible to prevent cells from becoming cancerous during cell proliferation and differentiation.

For the modeling aim, a novel scanning ion conductance microscopy technique has been reported in [15] for assessing the volume of living cells and the method gives a high-resolution characterization of dynamic changes in cell volume without change in cell functionality. Volume growth rate and division probability functions for mammalian cells have been determined as functions of cell volume [16], and

[a]e-mail: sharifi@qut.ac.ir

integral equations are derived from the distribution of birth volumes in successive generations [17]. Despite biological diversity, the dynamics of a single cell volume exhibit common basic features in various types of cells [18]. In some mathematical models [19], the surface S and volume V of a cell is considered as $S = \beta V^n$, $\beta > 0$, where β is a positive real number, and the main result is that the volume should grow at least with a third power of the time. In [20], a linear time increase for dry mass is found, while volume growth curves are either quadratic or exponential, depending on the relative contributions of metabolism and transport to cell water. An interesting side of cells' inherent biological processes is the beautiful physical geometry representations [21, 22]. Here, we will derive equations for cell radius more generally with physical insight and without assumption on the type of growth, i.e., spherical, linear, or exponential growth, and also the control action is taken into account.

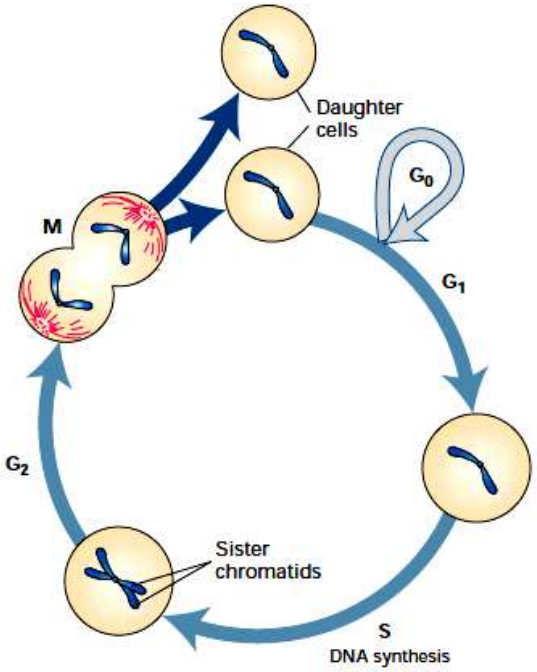

Fig. 1: Major phases of the cell cycle: G1 is the period between "birth" of a cell and the initiation of DNA synthesis. In the S phase, a replicated chromosome consists of two daughter DNA molecules, and associated chromosomal proteins (sister chromatid) will be produced. The end of G2 is marked by the onset of mitosis followed by the division of the cytoplasm to yield two daughter cells. The G1, S, and G2 phases are collectively referred to as interphase. The non-proliferating cells leave the cell cycle in G1 and enter the G0 state [13].

Assumptions and Notations

Let us define some notations used in this paper. We denote the mass and volume of a cell by m and V, respectively. The inner product between two vectors $\vec{A}$ and $\vec{B}$ is

$$\langle \vec{A}, \vec{B} \rangle = \vec{A} \cdot \vec{B}, \tag{1}$$

and $\|\vec{A}\| = \sqrt{\langle \vec{A}, \vec{A} \rangle}$ is the Euclidean norm. The vector $\vec{r}$ denotes the position vector. For instance, in spherical coordinates, $\vec{r} = (r, \theta, \varphi)$. For a scalar function $f(\vec{r}) = f(r, \theta, \varphi)$, one has

$$\nabla f = \partial_r f \, \hat{r} + \frac{1}{r} \partial_\theta f \, \hat{\theta} + \frac{1}{r \sin\theta} \partial_\varphi f \, \hat{\varphi}. \tag{2}$$

$$\nabla^2 f = \frac{1}{r^2} \partial_r \left(r^2 \partial_r f \right) + \frac{1}{r^2 \sin\theta} \partial_\theta \left(\sin\theta \, \partial_\theta f \right) + \frac{1}{r^2 \sin^2\theta} \partial_\varphi^2 f. \tag{3}$$

To develop a model for dynamic cell proliferation, we assume the following conditions:

1. The nutrition (mass) diffuses from a homogeneous medium into a cell and vice versa.
2. The temperature is constant and its variation is negligible.
3. The synthesis of cell mass involves the by-now-familiar processes of transcription and translation.
4. The mass and volume for some time interval are increasing, and in another interval are decreasing. The mass and volume are functions $m(t, \vec{r})$ and $V(t, \vec{r})$.

2 Proliferation Kinetics of Cell Mass Density and Radius

First of all, we visualize a single-parent cell with an arbitrary shape. It has a radius vector function $\vec{R}(t, \vec{r})$ and a mass density $\rho(t, \vec{r})$. The cell imports water and some chemical particles needed for growth and some biochemical reactions and other processes will occur. In physical view those processes have important consequences: the variation of volume and mass. Before the division starts time, the cell mass and volume increase. In the division phase, the parent cell growth will divide into daughter cells. To model this phase, we imagine that one daughter cell is a newly created parent cell that exports the second daughter cell like an ensemble of mass outside itself, see Fig. 2. Then with this idea, we can assume that we have two general physical phases in cell proliferation: first is the mass import and expansion, and the second is mass export and contraction.

Mass current and flow. The time rate of mass is called the mass current, i.e.

$$I_m = \frac{dm}{dt}. \tag{4}$$

The mass flux is defined as $J_m = I_m / A$, where A is the surface section of volume mass transit. If the direction of mass transit is denoted by $\vec{n}$, then $\vec{J}_m = J_m \vec{n}$ is the mass flow [23].

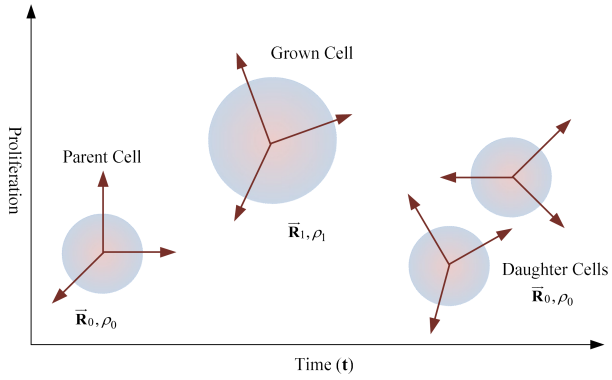

Fig. 2: A simple schematic that shows a mitosis cell division: in the initial time of growth the cell radius increases to a new radius, not equal to twice the initial radius, and then after some time when the division starts, the radius decreases to a new decreased radius for a cell.

Cell mass diffusion and Fick's laws. Molecules will move from where they are at a high concentration to where they are at a lower concentration. They diffuse down a concentration gradient. Fick's law is used to measure the rate of diffusion. The larger the area and difference in concentration cause thinner surface and quicker rate. By this law we have

$$\vec{J}_m + D\nabla\rho = 0, \tag{5}$$

where $\vec{J}_m$ is the mass current flow, D is the diffusion coefficient and $\rho(t,\vec{r})$ is the mass density. By using Fick's first law and the continuity equation, i.e.

$$\nabla\cdot\vec{J}_m + \partial_t\rho = 0, \tag{6}$$

one has the well-known Fick's second law of diffusion:

$$\partial_t\rho = -\nabla\cdot(D\nabla\rho). \tag{7}$$

For an isotropic diffusion coefficient, this equation reduces to

$$\partial_t\rho = -D\nabla^2\rho. \tag{8}$$

Force on the Cell Surface. Let $\vec{R} = \vec{R}(t,\vec{r})$ be the cell vector function at time t and in the direction $\vec{r}$. Let us define* $m_{\vec{R}} = c_1\rho\|\vec{R}\|$ as the mass distributed along the radius vector $\vec{R}$ in the cell, where c_1 is a dimensional correction constant. By Newton's second law, the force exerted along the vector $\vec{R}$ on the cell surface is

$$\vec{F} = \frac{d\vec{P}}{dt}, \tag{9}$$

*More generally, one may consider a nonlinear relation $m_{\vec{R}} = f(\rho)\|\vec{R}\|$, where $f(\rho)$ is a scalar nonlinear function. For simplicity, we restrict ourselves here to the linear case $f(\rho) = c_1\rho$.

where

$$\vec{P} = m_{\vec{R}}\partial_t\vec{R} = c_1\rho\|\vec{R}\|\partial_t\vec{R}. \tag{10}$$

Thus we arrive at†

$$\vec{F} = \partial_t\vec{P} = c_1\partial_t\left(\rho\|\vec{R}\|\partial_t\vec{R}\right). \tag{11}$$

Since the force $\vec{F}$ is proportional to the mass flow $\vec{J}_m$, then likewise by variation of mass, the force direction and amplitude will change. Hence, we postulate heuristically a law that relates the cell surface force with diffused mass‡.

The Cell Force–Mass Divergence Law: the force divergence is proportional to the intercellular mass density up to the transportability constant c:

$$\nabla\cdot\vec{F} = c\rho. \tag{12}$$

By using the force divergence law (12) together with Eq. (2), and the vector calculus identity [24]

$$\nabla\cdot(g\vec{A}) = \nabla g\cdot\vec{A} + g\nabla\cdot\vec{A}, \tag{13}$$

for the scalar $g = c_1\rho\|\vec{R}\|$ and the vector $\vec{A} = \partial_t\vec{R}$, we obtain

$$\begin{aligned}
&\partial_t\rho\,\|\vec{R}\|\nabla\cdot(\partial_t\vec{R}) + \rho\,\partial_t\|\vec{R}\|\nabla\cdot(\partial_t\vec{R})\\
&\quad+\rho\,\|\vec{R}\|\partial_t\nabla\cdot(\partial_t\vec{R})\\
&\quad+\nabla\left(\partial_t\rho\,\|\vec{R}\|\right)\cdot\partial_t\vec{R}\\
&\quad+\nabla\left(\rho\,\partial_t\|\vec{R}\|\right)\cdot\partial_t\vec{R} - k\rho = 0.
\end{aligned} \tag{14}$$

Here $k = c/c_1$. Equation (17) is a scalar equation; hence it does not directly determine the cell radius vector. The proof of this equation is as follows. From (11), one has

$$\vec{F} = \partial_t\vec{P} = \partial_t\left(c_1\rho\|\vec{R}\|\partial_t\vec{R}\right). \tag{15}$$

$$\begin{aligned}
\nabla\cdot\vec{F} &= \nabla\cdot\left(\partial_t\vec{R}\,\partial_t(c_1\rho\|\vec{R}\|) + c_1\rho\|\vec{R}\|\,\partial_t^2\vec{R}\right)\\
&= \left\langle\nabla(c_1\rho\|\vec{R}\|),\partial_t^2\vec{R}\right\rangle\\
&\quad+\left\langle\nabla\left(\partial_t(c_1\rho\|\vec{R}\|)\right),\partial_t\vec{R}\right\rangle\\
&\quad+\partial_t(c_1\rho\|\vec{R}\|)\nabla\cdot(\partial_t\vec{R})\\
&\quad+c_1\rho\|\vec{R}\|\nabla\cdot(\partial_t^2\vec{R}) = c\rho.
\end{aligned} \tag{16}$$

†Since $\vec{P} = c_1\rho(t,\vec{r})\,\|\vec{R}(t,\vec{r})\|\,\partial_t\vec{R}(t,\vec{r}) = \vec{P}(t,\vec{r})$ and $\vec{r}$ does not depend on time, $\partial_t\vec{r} = 0$, the total time derivative of $\vec{P}$ reduces to the partial time derivative:

$$\frac{d\vec{P}}{dt} = \frac{\partial\vec{P}}{\partial t} + \frac{\partial\vec{P}}{\partial\vec{r}}\cdot\frac{\partial\vec{r}}{\partial t} = \frac{\partial\vec{P}}{\partial t}.$$

‡This law is the analogue of Gauss' divergence law for the electric displacement field $\vec{D}$ and charge density ρ [24], namely $\nabla\cdot\vec{D} = \rho$.

Since $\nabla\cdot\vec{F}=c\rho$, one has

$$\left\langle\nabla\left(c_1\rho\|\vec{R}\|\right),\partial_t^2\vec{R}\right\rangle+\left\langle\nabla\left(\partial_t\rho\,\|\vec{R}\|\right),\partial_t\vec{R}\right\rangle + \partial_t\rho\,\|\vec{R}\|\nabla\cdot(\partial_t\vec{R})+\rho\|\vec{R}\|\nabla\cdot(\partial_t^2\vec{R})-k\rho=0. \tag{17}$$

where $k=c/c_1$, and the proof is complete. To obtain the radius vector, we have to extract a vector partial differential equation. Note that

$$\partial_t(\nabla\cdot\vec{F})=\nabla\cdot\partial_t\vec{F}=\nabla\cdot\partial_t^2\left(c_1\rho\|\vec{R}\|\partial_t\vec{R}\right)=c\,\partial_t\rho. \tag{18}$$

Since ∂_t and ∇ are continuous operators, and since ρ and $\vec{R}$ are continuous functions, the operators ∂_t and ∇ commute:

$$[\partial_t,\nabla]=\partial_t\nabla-\nabla\partial_t=0. \tag{19}$$

By substituting from Eq. (7) for $\partial_t\rho$, one finds

$$\nabla\cdot\partial_t^2\left(c_1\rho\|\vec{R}\|\partial_t\vec{R}\right)=-\nabla\cdot(cD\nabla\rho), \tag{20}$$

or equivalently

$$\nabla\cdot\left[\partial_t^2\left(c_1\rho\|\vec{R}\|\partial_t\vec{R}\right)+cD\nabla\rho\right]=0. \tag{21}$$

Thus, the expression inside the divergence is a vector independent of the spatial coordinates. Therefore,

$$\partial_t^2\left(\rho\|\vec{R}\|\partial_t\vec{R}\right)+(kD)\nabla\rho=\alpha\vec{u}(t)+\vec{v}. \tag{22}$$

For a general function $m_{\vec{R}}=f(\rho)\|\vec{R}\|$, Eq. (22) becomes

$$\partial_t^2\left(f(\rho)\|\vec{R}\|\partial_t\vec{R}\right)+(kD)\nabla\rho=\alpha\vec{u}(t)+\vec{v}. \tag{23}$$

The vector $\alpha\vec{u}(t)+\vec{v}$ is interpreted as a control action regulating cell proliferation. Here α and $\vec{v}$ are, respectively, a constant scalar and a constant vector. For instance, the control signals of these events are a small number of heterodimeric protein kinases containing a regulatory subunit, called cyclin, and a catalytic subunit, called cyclin-dependent kinase. These kinases regulate the activities of multiple proteins; for more details, see [13]. The solution of the partial differential equations (7) and (22) gives the time evolution of the cell radius and mass density. By appropriate control, the regulation of proliferation toward the true profile becomes possible.

3 Analysis of the Cell Mass-Volume Diffusion Dynamic

Consider the mass-volume relation $m=\rho V$ and the mass rate $\partial_t m$. By Eq. (7) for constant diffusion, we obtain

$$\frac{\partial_t m}{m}-\frac{\partial_t V}{V}=-D\left(\frac{\nabla^2V}{V}-2\frac{\|\nabla V\|^2}{V^2}\right), \tag{24}$$

where $\nabla^2V=\partial_x^2V+\partial_y^2V+\partial_z^2V$ is the Laplace operator in Cartesian coordinates and

$$\|\nabla V\|^2=(\nabla V,\nabla V)=(\partial_xV)^2+(\partial_yV)^2+(\partial_zV)^2. \tag{25}$$

Based on the last equation, we have these conditions.

(a) The first phase of proliferation, the cell grows. In this phase, both the mass amount and the volume are increasing and hence $\partial_tV,\partial_tm>0$, but evidence shows that the mass increase ratio is more than the volume increase ratio [23], i.e.

$$\frac{\partial_t m}{m}>\frac{\partial_t V}{V}>0. \tag{26}$$

Then one finds for volume the relation

$$V(\partial_xV)^2+V(\partial_yV)^2+V(\partial_zV)^2 - 2\partial_x^2V-2\partial_y^2V-2\partial_z^2V<0. \tag{27}$$

(b) At t_0,

$$\frac{\partial_t m}{m}=\frac{\partial_t V}{V}, \tag{28}$$

which means the cell stops growing. For $t>t_0$ the cell starts to divide, and in the division phase we have $V,m>0$ and $\partial_tV,\partial_tm<0$. Also

$$\frac{\partial_t m}{m}<\frac{\partial_t V}{V}<0, \tag{29}$$

which is equivalent to $\partial_t\rho<0$ or $\nabla\cdot\vec{J}_m>0$, which means that the mass flows outward the cell.

Remark. During a normal exponential-growth cell cycle, both DNA content N and the cytoplasmic mass C double, but asynchronously. In the cell cycle and after mitosis, the cells begin to increase C, thus late G1 cells have a low N/C ratio. In the subsequent step, S-phase, the nucleus content of the cells doubles, thus the $N/C\simeq 1$ is re-established [25]. According to our model, when the volume growth rate of the cell, increase in cytoplasm, is equal to its mass growth rate, increase in nuclear mass, the cell will divide.

4 Conclusion

Here, we derive some partial differential equations for radius vector and mass density of a cell. The systematic views of biological processes are still in their infancy; it is far from clear at this time what will be the ultimate impact of systematic view of cell growth, symmetric and asymmetric. As a future work, someone can model the asymmetric cell proliferation and differentiation.

References

1. M. B. Elowitz and S. Leibler, Nature, vol. 403, no. 20, pp. 335–338, 2000. DOI: https://doi.org/10.1038/35002125

2. L. Chen and K. Aihara, IEEE Transactions on Circuits and Systems, vol. 49, no. 10, 2002. DOI: https://doi.org/10.1109/TCSI.2002.803354
3. B. S. Chen and Y. C. Wang, BMC Bioinformatics, 7, 52, doi:10.1186/1471-2105-7-52, 2006. DOI: https://doi.org/10.1186/1471-2105-7-52
4. R. Jothi et al., Molecular Systems Biology, vol. 5, doi:10.1038/msb.2009.52, 2009. DOI: https://doi.org/10.1038/msb.2009.52
5. R. Siammas et al., Molecular Systems Biology, vol. 7, no. 25, 2011. DOI: https://doi.org/10.1038/msb.2011.25
6. T. S. Gardner, C. R. Cantor and J. J. Collins, Nature, vol. 403, no. 20, pp. 339–342, 2000. DOI: https://doi.org/10.1038/35002131
7. V. A. Rhodius et al., Molecular Systems Biology, vol. 9, doi:10.138/msb.2013.58, 2013. DOI: https://doi.org/10.1038/msb.2013.58
8. L. M. Adleman, Science, 266, 5187, pp. 1021–1024, 1994. DOI: https://doi.org/10.1126/science.7973651
9. Y. Benenson et al., Nature, 414, 6862, pp. 430–434, 2001. DOI: https://doi.org/10.1038/35106533
10. M. N. Stojanovic, T. E. Mitchell and D. Stefanovic, Journal of the American Chemical Society, 124, 14, pp. 3555–3561, 2002. DOI: https://doi.org/10.1021/ja016756v
11. J. I. Farren, J. Hasty, C. R. Cantor and J. J. Collins, PNAS, vol. 100, no. 13, pp. 7714–7719, 2003. DOI: https://doi.org/10.1073/pnas.1332628100
12. J. MacDonald et al., Nano Letters, vol. 6, no. 11, pp. 2598–2603, 2006. DOI: https://doi.org/10.1021/nl0620684
13. H. Lodish et al., *Molecular Cell Biology*, sixth edition, W. H. Freeman, 2007.
14. M. Gthocleous and W. Harris, Trends in Cell Biology, vol. 23, no. 10, pp. 484–491, 2013. DOI: https://doi.org/10.1016/j.tcb.2013.05.004
15. Y. E. Korchev et al., Biophysical Journal, 78, 1, pp. 451–457, 2000. DOI: https://doi.org/10.1016/S0006-3495(00)76605-7
16. W. B. Bonnor, Bulletin of Mathematical Biology, 29, 3, pp. 429–436, 1967. DOI: https://doi.org/10.1007/BF02476582
17. E. C. Anderson et al., Biophysical Journal, 9, 2, pp. 246–263, 1969. DOI: https://doi.org/10.1016/S0006-3495(69)86383-6
18. G. I. Bell, Biophysical Journal, 8, 4, pp. 431–444, 1968. DOI: https://doi.org/10.1016/S0006-3495(68)86498-7
19. U. C. Selhuber et al., Physical Biology, 6, 2, 025015, 2009. DOI: https://doi.org/10.1088/1478-3975/6/2/025015
20. J. A. Hernandez, Bulletin of Mathematical Biology, 69, 5, pp. 1631–1648, 2007. DOI: https://doi.org/10.1007/s11538-006-9181-5
21. M. Terasaka et al., Cell, vol. 154, no. 2, pp. 285–296, 2013. DOI: https://doi.org/10.1016/j.cell.2013.06.043
22. F. M. Wallas, Cell, vol. 154, issue 2, pp. 265–266, 2013. DOI: https://doi.org/10.1016/j.cell.2013.06.044
23. M. Potter and D. C. Wiggart, *Fluid Mechanics*, McGraw-Hill, 2008.
24. T. Chow, *Mathematical Methods for Physicists: A Concise Introduction*, Cambridge University Press, 2003.
25. D. H. Worthington, M. Salamone and D. S. Nachtwey, Cell Proliferation, vol. 9, 2, pp. 119–130, 1976. DOI: https://doi.org/10.1111/j.1365-2184.1976.tb01260.x

TTMP vol 3 (1), 2026
doi: 10.30511/TTMP.2026.2076630.1066

Transactions in Theoretical and Mathematical Physics

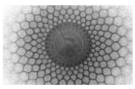

Extended GZK Cutoff in Momentum-Curved Space via Modified Dispersion Relations

Sanaz Safarian[1], **Zahra Norouzbeh**[1], **Mehdi Jafari Matehkolaee**[a,2]

[1]Department of Physics, Faculty of Physics & Chemistry, Alzahra University, Tehran, Iran
[2]Department of Physics and Energy Engineering, Amirkabir University of Technology (Tehran Polytechnic), Hafez Avenue, Tehran, Iran

Received: 03 November 2025 / Accepted: 03 February 2026 / Published: 27 February

Abstract

We extend the Greisen–Zatsepin–Kuzmin (GZK) cutoff within a momentum-curved space framework derived from a specific modified dispersion relation (MDR) inspired by doubly special relativity (DSR). Our formulation yields an extended GZK equation suggesting that ultra-high-energy cosmic rays (UHECRs) can exceed the conventional limit of 10^{20} eV, consistent with recent experimental results. This provides a phenomenological link between Planck-scale deformations of space-time symmetries and observable cosmic-ray phenomena.

1 Introduction

In Einstein's theory of special relativity, the speed of light is a universal quantity and a fundamental constant of nature, invariant under Lorentz transformations among inertial observers. On the other hand, quantum gravity theories suggest the existence of a minimum length. Based on the definition of this length, it should be a universal quantity and therefore the same for all observers. However, in the framework of special relativity, any length under Lorentz transformations between observers undergoes Lorentz–FitzGerald contraction, so this theory does not predict any universal length. According to this, a redefinition of Lorentz transformations is necessary so that all observers agree on the existence of a global minimum length.

The idea of this theory was proposed in the early twenty-first century [1]. This theory is called doubly, or deformed, special relativity because, in addition to the speed of light, a minimum length remains unchanged under transformations between observers. In the first model presented by Amelino-Camelia, Lorentz symmetry was considered as an approximate symmetry that is broken in the high-energy regime and valid only in the normal energy regime. Almost a year after this model was introduced, doubly special relativity was formulated in such a way that Lorentz symmetry was preserved even at high energies [2]. However, it is clear that the validity of Lorentz symmetry in the high-energy regime of the order of the Planck scale can only be achieved by experiment. Finally, it was found that there is no unique doubly special relativity, but rather an infinite number of DSR theories, among which there is no special superiority because there is no authentic physical reason for distinction and preference between them.

In this paper, we examine the GZK paradox for ultra-high-energy cosmic rays in momentum-curved space. This paradox arises because some ultra-high-energy cosmic rays with energies exceeding this limit have been observed [3]. This discrepancy raises questions about the sources of these cosmic rays and the mechanisms involved in their propagation through the universe [4]. After introducing the MDR model in Sect. 2, we analyze the generalized GZK equation in momentum-curved space in Sect. 3.

2 Non-commutativity of space-time and momentum-curved space

In the first model of doubly special relativity, Lorentz transformations were generalized in such a way that, in addition to the speed of light, a minimum length remains invariant under transformations between observers. Lorentz symmetry in this initial model was broken at high energies [1]. Shortly after the presentation of this model, two general results were obtained: first, with the nonlinear action of the Lorentz group on momentum space, a model of DSR can be presented in which Lorentz symmetry is not broken but generalized [2]; second, there is an infinity of doubly special

[a]m.matehkolaee@aut.ac.ir

relativity theories [5]. The momentum space in these models is a curved de Sitter space [5], and different DSR models correspond to different definitions of energy and momentum on this curved space.

Noncommutative space-time is a general consequence of theories and models of quantum gravity which indicate the existence of a minimal length. In a general and mathematical sense, non-commutativity between the variables of a space indicates the curvedness of the space of dependent conjugate variables [6]. This concept also exists in the theory of general relativity. In this theory, based on the equivalence principle, gravity is considered as the curvature of space-time, and therefore the space of conjugate variables, namely momentum space, is a noncommutative space. More precisely, the covariant derivatives, which are the generators of translations in curved space-time, do not commute with each other, and their noncommutativity is related to the Riemann tensor, which measures the intrinsic curvature of space-time.

We know special relativity as a non-gravitational theory, and therefore, within this framework, space-time is flat. Also, in doubly special relativity, space-time is flat, but space-time variables are noncommutative. In a four-dimensional momentum space, space-time variables and momenta are conjugate to each other. Hence, just as in general relativity the non-commutativity of momentum corresponds to the curvature of space-time, in DSR the non-commutativity of space-time indicates the curvature of momentum space. In this way, within the framework of special relativity, momentum space must be curved.

In general relativity, the curvature of space-time, for example even for a static gravitational field, is a function of the space-time coordinates. But in DSR, the existence of a global minimal length causes momentum space to be curved. Since all observers must agree on the size of this length, the curvature of momentum space in DSR is necessarily constant. On the other hand, spaces with constant curvature are also spaces with maximum symmetry [6]. Due to the Lorentzian nature of the space in relativity, there are only two choices for the curved momentum space with constant curvature, which are de Sitter and anti-de Sitter spaces.

Regardless of whether we look at DSR models from an algebraic or geometric point of view, or whether momentum space is de Sitter or anti-de Sitter, all models eventually lead to a modified dispersion relation. The general form of these modified dispersion relations is

$$f^2(\lambda E)E^2 - g^2(\lambda E)P^2 = m^2, \tag{1}$$

where m is the mass, and f and g are functions of energy that differ from one model to another. Based on the correspondence principle, the results of special relativity should be recovered in the low-energy regime, so for all models one has

$$\lim_{\lambda E\to 0} f(\lambda E) = 1, \qquad \lim_{\lambda E\to 0} g(\lambda E) = 1. \tag{2}$$

In this paper, the model used is

$$\left(\frac{2}{\lambda}\sinh\frac{\lambda E}{2}\right)^2 - e^{\lambda E}p^2 = m^2, \tag{3}$$

where λ is the quantum deformation parameter [7]. The energy-momentum variables (E,p) live on a manifold with de Sitter geometry [5, 7], while space-time is flat. The modified dispersion relation used in this work should be understood as a phenomenological realization inspired by DSR models with curved de Sitter momentum space. In the low-energy limit $\lambda E \ll 1$, it reduces to the standard special relativistic dispersion relation, ensuring consistency with known physics. In this study, the deformation parameter λ is treated as an effective Planck-scale parameter of order $E_{\rm Pl}^{-1}$.

3 Extended GZK cutoff

In our previous work [8], we have shown the effects of modified dispersion relations and Lorentz invariance violation on inverse Compton scattering of CMB photons and on the GZK cutoff. For the Compton effect, our results are exactly compatible with the analyzed model in Ref. [8], by setting $n = 2$.

We use natural units $c = 1$ and the metric signature $(-,+,+,+)$. A representative CMB photon energy $\varepsilon \simeq 10^{-3}\,\text{eV}$ is adopted for threshold estimates. We consider the reaction between cosmic-ray protons, namely high-energy protons, and CMB photons,

$$p + \gamma \longrightarrow n + \pi^+. \tag{4}$$

The positively charged pion ensures charge conservation. Since the square of the total four-momentum is invariant, namely the Casimir associated with the adopted modified dispersion relation, any inertial observer obtains the same value for it. In the following derivation, we adopt the modified dispersion relation while keeping the standard additive energy-momentum conservation law. This approximation allows us to isolate the effect of the MDR on the threshold condition. Possible modifications of momentum composition, which may arise in a fully deformed DSR framework, are left for future investigation.

Thus, we obtain

$$(\mathscr{P}_p + \mathscr{P}_\gamma)^2 = (\mathscr{P}_n + \mathscr{P}_\pi)^2, \tag{5}$$

which can also be written as

$$\mathscr{P}_p^2 + 2\mathscr{P}_p\cdot\mathscr{P}_\gamma + \mathscr{P}_\gamma^2 = -(m_n + m_\pi)^2c^2. \tag{6}$$

For a particle with total energy E and momentum $\vec{p}$, the four-momentum is written as

$$\mathscr{P} = \left(\frac{E}{c}, \vec{p}\right), \tag{7}$$

and the square of the four-momentum is defined as

$$\mathscr{P}^2 = \mathscr{P} \cdot \mathscr{P} = -m^2c^2. \tag{8}$$

From the above relation and Eq. (4), we get

$$\mathscr{P}_p^2 = -m_p^2c^2 + \frac{\lambda^2}{12}p_p^4. \tag{9}$$

Putting Eq. (9) into Eq. (8), one obtains

$$\left(\frac{m_n^2c^4 - m_p^2c^4 + m_\pi^2c^4}{4E_\gamma}\right) = E_p + \frac{\lambda^2}{12}\frac{E_p^4}{4E_\gamma}. \tag{10}$$

The neutron mass is

$$m_nc^2 \simeq 939.6\,\mathrm{MeV}, \tag{11}$$

and that of the π^+ meson is

$$m_\pi c^2 \simeq 139.6\,\mathrm{MeV}. \tag{12}$$

Taking $E_\gamma = 1.1\,\mathrm{meV}$ for the energy of the cosmic microwave background photon, we obtain

$$E_p = 3 \times 10^{20}\,\mathrm{eV} + \frac{\lambda^2}{12}\frac{E_p^4}{4E_\gamma}. \tag{13}$$

In deriving the modified threshold condition, we work in the high-energy regime $E_p \gg m_pc^2$ and retain leading-order terms in the deformation parameter λ. Subleading terms are neglected. In the limit $\lambda \to 0$, the standard GZK threshold is recovered. Obviously, Eq. (13) indicates that

$$E_p > 10^{20}\,\mathrm{eV}. \tag{14}$$

This result, similar to the extended Compton effect, is completely consistent with Ref. [8]. According to Eq. (13), if λ tends to zero, then the common GZK cutoff is obtained.

Current observations [3, 9–11] indicate an overall suppression of the UHECR spectrum at the highest energies, while rare events above $10^{20}\,\mathrm{eV}$ continue to motivate investigations of possible deviations from standard kinematics.

4 Conclusion

Doubly special relativity provides a framework to reconcile Planck-scale effects with relativistic invariance. Within this setting, we have derived an extended GZK cutoff using a modified dispersion relation in momentum-curved space. Our results demonstrate that high-energy cosmic rays may surpass the standard GZK limit, consistent with current experimental trends. This reinforces the potential role of Planck-scale physics in observable astrophysical phenomena [12].

In our opinion, further work may focus on the following directions:

1) exploring anisotropies in momentum-curved space and their influence on cosmic-ray propagation;
2) comparing predictions with updated Auger and Telescope Array data through numerical modeling;
3) extending the MDR framework to neutrino oscillations and photon dispersion;
4) linking DSR-based MDRs with loop quantum gravity or κ-Minkowski space-time models.

References

1. G. Amelino-Camelia, Relativity in space-times with short-distance structure governed by an observer-independent (Planckian) length scale, Int. J. Mod. Phys. D **11**, 35–59 (2002). DOI: https://doi.org/10.1142/S0218271802001330
2. J. Magueijo and L. Smolin, Generalized Lorentz invariance with an invariant energy scale, Phys. Rev. D **67**, 044017 (2003). DOI: https://doi.org/10.1103/PhysRevD.67.044017
3. N. Hayashida, K. Honda, M. Honda, S. Imaizumi, N. Inoue, K. Kadota, F. Kakimoto, S. Kawaguchi, et al., Phys. Rev. Lett. **73**, 3491 (1994). DOI: https://doi.org/10.1103/PhysRevLett.73.3491
4. R. A. Batista, J. Biteau, M. Bustamante, et al., Open questions in cosmic-ray research at ultrahigh energies, Front. Astron. Space Sci. **6**, 23 (2019). DOI: https://doi.org/10.3389/fspas.2019.00023
5. J. Kowalski-Glikman, De Sitter space as an arena for doubly special relativity, Phys. Lett. B **547**, 291–296 (2002). DOI: https://doi.org/10.1016/S0370-2693(02)02755-4
6. S. Majid, Meaning of noncommutative geometry and the Planck-scale quantum group, Lect. Notes Phys. **541**, 227–276 (2000). DOI: https://doi.org/10.1007/3-540-46637-1_9
7. L. Barcaroli, L. K. Brunkhorst, G. Gubitosi, N. Loret and C. Pfeifer, Planck-scale-modified dispersion relations in homogeneous and isotropic space-times, Phys. Rev. D **95**, 024036 (2017). DOI: https://doi.org/10.1103/PhysRevD.95.024036
8. A. Majidian and M. Jafari Matehkolaee, GZK cutoff in presence of a specified modified dispersion relation, Gravit. Cosmol. **29**, 432–436 (2023). DOI: https://doi.org/10.1134/S0202289323040097
9. K. Shinozaki and M. Teshima, AGASA Collaboration, Nucl. Phys. Proc. Suppl. **136**, 18 (2004). DOI: https://doi.org/10.1016/j.nuclphysbps.2004.10.003
10. F. Stecker, Revisiting the GZK cutoff in light of Auger and TA data, Astropart. Phys. **159**, 103082 (2024). DOI: https://doi.org/10.1016/j.astropartphys.2024.103082

11. M. Unger et al., Recent results from the Pierre Auger Observatory on UHECR spectrum and composition, Front. Phys. **13**, 145671 (2024). DOI: https://doi.org/10.22323/1.476.0678

12. G. Amelino-Camelia, Planck-scale relativity after two decades: progress and open questions, Universe **10** (2024). DOI: https://doi.org/10.3390/universe10010016

TTMP vol 3 (1), 2026
doi: 10.30511/TTMP.2026.2087308.1073

Transactions in Theoretical and Mathematical Physics

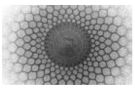

Balance Laws and Soliton Persistence in a Nonlinear Schrödinger Equation with Delayed Kerr Response

A. Latifi[1,a], **E. Namvar**[1]

[1] Department of Mechanics, Qom University of Technology, Qom, Iran

Received: 22 January 2026 / Accepted: 08 February 2026 / Published: 27 February 2026

Abstract We study the persistence and slow evolution of soliton solutions of a nonlinear Schrödinger equation perturbed by a nonlinear intensity–gradient term arising from a weakly noninstantaneous Kerr response. Starting from Maxwell's equations with a nonlocal nonlinear polarization, we derive a perturbed envelope equation containing the correction $i\eta\,\psi\,\partial_t|\psi|^2$, which represents the leading contribution of a short-memory nonlinear response. To analyze the resulting dynamics we employ a variational collective–coordinate reduction that describes the pulse in terms of a small set of evolving soliton parameters. The reduced dynamical system shows that the perturbation preserves the optical power while producing a slow evolution of the soliton center and carrier frequency. At the level of the governing partial differential equation we derive an exact balance law for the momentum, which reveals that the nonlinear gradient term acts as a systematic source of momentum drift. This balance relation yields explicit scaling predictions for the long-distance evolution of the soliton parameters. Numerical simulations confirm the persistence of a localized pulse together with the predicted parameter drift. The results provide a transparent connection between the microscopic origin of delayed nonlinear responses, the modified conservation structure of the perturbed equation, and the observable dynamics of optical solitons.

Keywords: nonlinear Schrödinger equation, optical solitons, delayed Kerr response, balance laws, collective coordinates.

1 Introduction

Localized nonlinear wave packets play a fundamental role in many areas of modern physics, ranging from fluid dynamics and plasma physics to nonlinear optics and Bose–Einstein condensates. Among the most prominent examples are optical solitons, which arise when the dispersive spreading of a pulse is exactly balanced by nonlinear self–phase modulation in a Kerr medium. This balance leads to robust, shape–preserving propagation and provides the basis for a wide range of physical phenomena. The theoretical description of such pulses is most commonly formulated in terms of the nonlinear Schrödinger equation (NLSE), which serves as a universal envelope equation for weakly nonlinear dispersive waves [1–3].

The NLSE occupies a distinguished position in nonlinear science because it is both physically relevant and mathematically integrable. Its soliton solutions were first obtained through the inverse scattering method by Zakharov and Shabat [4], establishing the NLSE as a prototype integrable nonlinear wave system. Shortly thereafter, Hasegawa and Tappert demonstrated that the same equation governs the propagation of optical pulses in dispersive dielectric fibers, providing the first experimental platform for NLSE soliton dynamics [5, 6]. Classical treatments of NLSE theory and applications can be found in [1, 2, 7–10].

In realistic optical media, however, the nonlinear response is not strictly instantaneous. The Kerr response originates from electronic and molecular polarization processes with finite relaxation times, and therefore the nonlinear polarization may depend not only on the instantaneous intensity but also on its temporal variation. This behavior is naturally modeled using a nonlocal response function [10]. When the response time is short compared with the pulse duration, a systematic expansion of the response kernel yields higher–order corrections to the standard Kerr model. Of particular interest is a nonlinear intensity–gradient term of the form $i\eta\,\psi\,\partial_t|\psi|^2$, which arises in several nonlocal and delayed–response models.

[a]e-mail: latifi@qut.ac.ir

Such perturbations break the integrability of the NLSE and lead to a slow evolution of the soliton parameters along the propagation direction. The resulting solitary waves are no longer exact solitons but slowly varying structures whose amplitude, width, frequency, and center evolve during propagation. Early systematic methods for analyzing these effects relied on perturbation theory and inverse scattering [11, 12]. Variational approaches [13, 14] provide a complementary framework in which the pulse is represented by a parameterized ansatz, reducing the NLSE dynamics to a finite–dimensional system for the soliton parameters.

In the last few years there has been renewed interest in perturbations of the NLSE generated by delayed, nonlocal, and ultrafast nonlinear responses. These effects are especially important in modern platforms such as photonic crystal fibers, integrated waveguides, and ultrafast nonlinear media. Recent studies have investigated how weak nonlocal corrections and delayed Kerr responses influence soliton stability, parameter drift, and modified conservation laws [15–18]. Broader perspectives on noninstantaneous effects and generalized NLSE models in contemporary optics are provided in recent works [19, 20].

Motivated by these developments, this paper analyzes the persistence and slow evolution of NLSE solitons in the presence of a nonlinear intensity–gradient perturbation. Starting from Maxwell's equations with a nonlocal nonlinear polarization, we derive a perturbed NLSE that incorporates this correction. A variational collective–coordinate reduction is then used to obtain a dynamical system for the soliton parameters, enabling a clear characterization of the parameter drift induced by the perturbation.

A central goal of the analysis is to understand how the nonlinear gradient term modifies the conservation structure of the NLSE. We show that while the optical power remains conserved, the momentum satisfies a modified balance law that generates a monotonic drift of the soliton center and carrier frequency. The theoretical predictions are supported by numerical simulations, which illustrate the propagation dynamics and confirm the scaling behavior deduced from the balance law.

The remainder of the paper is organized as follows. Section 1 derives the perturbed NLSE from Maxwell's equations using a nonlocal nonlinear response model. Section 2 develops the variational formulation and obtains the equations governing the soliton parameters. Section 3 discusses soliton persistence and qualitative features, along with the physical interpretation of the gradient correction. Section 4 presents the balance laws and their implications for parameter drift. Section 5 provides numerical simulations validating the analytical predictions. Section 6 concludes with a discussion and outlook.

2 Physical Model and Governing Equations

We consider the propagation of an optical pulse in a weakly nonlinear, single-mode Kerr fiber. The starting point is Maxwell's equations in the absence of free charges and currents. For a nonmagnetic dielectric the electric displacement is

$$\mathbf{D} = \varepsilon_0 \mathbf{E} + \mathbf{P}, \tag{1}$$

where $\mathbf{P}$ denotes the material polarization. In nonlinear optics $\mathbf{P}$ is expressed as a power series in the electric field,

$$\mathbf{P} = \varepsilon_0 \left(\chi^{(1)} \mathbf{E} + \chi^{(2)} \mathbf{E}^2 + \chi^{(3)} \mathbf{E}^3 + \cdots \right), \tag{2}$$

with $\chi^{(n)}$ the nth-order electric susceptibilities [10]. In centrosymmetric media such as silica fibers, $\chi^{(2)} = 0$, so the leading nonlinear response arises from the third-order susceptibility. The corresponding Kerr polarization is

$$\mathbf{P}_{\mathrm{NL}} = \varepsilon_0 \chi^{(3)} |\mathbf{E}|^2 \mathbf{E}. \tag{3}$$

Substituting this expression into Maxwell's equations yields the nonlinear wave equation

$$\nabla^2 \mathbf{E} - \frac{n^2}{c^2} \frac{\partial^2 \mathbf{E}}{\partial t^2} = \frac{1}{\varepsilon_0 c^2} \frac{\partial^2 \mathbf{P}_{\mathrm{NL}}}{\partial t^2}, \tag{4}$$

where the linear index satisfies $n^2 = 1 + \chi^{(1)}$.

In a single-mode optical fiber the electric field is represented as

$$\mathbf{E}(x,y,z,t) = F(x,y)\, E(z,t)\, \hat{\mathbf{e}}, \tag{5}$$

where $F(x,y)$ is the normalized transverse mode profile, $\hat{\mathbf{e}}$ is the unit polarization vector, z is the propagation distance, and t denotes the laboratory time. Projecting Maxwell's equations onto the fundamental guided mode yields an effective one-dimensional evolution equation for the longitudinal field envelope $E(z,t)$.

Introducing a slowly varying complex envelope $\psi(z,T)$ via

$$E(z,t) = \frac{1}{2} \left[\psi(z,T)\, e^{i(k_0 z - \omega_0 t)} + \psi^*(z,T)\, e^{-i(k_0 z - \omega_0 t)} \right], \tag{6}$$

where ω_0 is the carrier angular frequency, $k_0 = \beta(\omega_0)$ is the corresponding propagation constant, and $T = t - z/v_g$ is the retarded time in a frame moving with the group velocity $v_g = (d\beta/d\omega)^{-1}|_{\omega_0}$, one expands the propagation constant $\beta(\omega) = n(\omega)\omega/c$ about ω_0. Retaining terms up to second order in the dispersion and applying the slowly varying envelope approximation leads to the nonlinear Schrödinger equation

$$i \frac{\partial \psi}{\partial z} + \frac{\beta_2}{2} \frac{\partial^2 \psi}{\partial T^2} + \gamma |\psi|^2 \psi = 0, \tag{7}$$

where $\beta_2 = d^2\beta/d\omega^2|_{\omega_0}$ is the group-velocity-dispersion coefficient and

$$\gamma = \frac{3\omega_0\chi^{(3)}}{8n^2(\omega_0)c} \tag{8}$$

is the Kerr nonlinearity parameter. Standard derivations of Eq. (7) for optical fibers may be found in Refs. [5–7, 21, 22].

Equation (7) admits localized solutions in the anomalous dispersion regime $\beta_2 < 0$, where the effects of dispersion and Kerr nonlinearity exactly balance. The fundamental bright soliton solution is

$$\psi(z,T) = A_0\,\mathrm{sech}\left(\frac{T}{T_0}\right)\exp\left(i\frac{\gamma A_0^2}{2}z\right), \tag{9}$$

where A_0 is the peak field amplitude and T_0 is the pulse width. These parameters satisfy the soliton condition $A_0^2T_0^2 = |\beta_2|/\gamma$. Defining the peak power $P_0 = A_0^2$, the dimensionless soliton order

$$S^2 = \frac{\gamma P_0 T_0^2}{|\beta_2|} \tag{10}$$

identifies the case $S = 1$ as the fundamental soliton [7].

Realistic dielectric materials may exhibit a weakly delayed Kerr response: the nonlinear refractive index depends not only on the instantaneous intensity but also on its temporal variation. Retaining the first-order term in this nonlocal expansion gives $n_{\mathrm{NL}} = n_2|\psi|^2 + \eta\,\partial_T|\psi|^2$, where the small parameter η characterizes the strength of the delay. Substitution into Eq. (7) yields the perturbed envelope equation

$$i\psi_z + \frac{\beta_2}{2}\psi_{TT} + \gamma|\psi|^2\psi = i\varepsilon\eta\,\psi\,\partial_T|\psi|^2, \tag{11}$$

with $0 < \varepsilon \ll 1$ emphasizing that the correction is weak. The added term introduces a nonlinear intensity-gradient perturbation that accumulates over long propagation distances and modifies the soliton parameters.

For subsequent analysis we normalize the equation using $\tau = T/T_0$, $\xi = z/L_D$, and $\psi = \sqrt{P_0}\,u(\xi,\tau)$, with dispersion length $L_D = T_0^2/|\beta_2|$ and soliton power $P_0 = |\beta_2|/(\gamma T_0^2)$. The resulting dimensionless form is

$$iu_\xi + \tfrac{1}{2}u_{\tau\tau} + |u|^2u = i\tilde{\eta}\,u\,\partial_\tau|u|^2, \tag{12}$$

where $\tilde{\eta} = \varepsilon\eta P_0 L_D/T_0$ quantifies the normalized perturbation strength. For $\tilde{\eta} = 0$ the fundamental soliton is $u(\xi,\tau) = \mathrm{sech}(\tau)e^{i\xi/2}$, while the small nonlinear gradient term introduces a slow, symmetry-breaking drift that will be examined analytically in subsequent sections.

3 Variational formulation and collective–coordinate dynamics

The perturbed propagation model introduced in Sec. 2 reduces to the standard nonlinear Schrödinger equation (NLSE) (7) in the absence of the nonlinear gradient term. While the NLSE is a completely integrable system possessing an infinite hierarchy of conservation laws and exact soliton solutions [4, 7], the additional perturbation breaks integrability and modifies the evolution of the pulse. When the perturbation strength is sufficiently small, however, solutions remain close to the fundamental soliton (9), and the optical pulse preserves its localized shape while its physical parameters vary slowly along the propagation coordinate z. Such slow modulations can be described efficiently through a reduced dynamical system for a finite set of collective variables characterizing the soliton [12, 13, 23].

The collective–coordinate approach exploits the Lagrangian structure of the unperturbed NLSE. Equation (7) follows from the stationary action principle $\delta S = 0$ with action $S = \int L\,dz$ and Lagrangian density

$$\mathscr{L} = \frac{i}{2}\left(\psi\psi_z^* - \psi^*\psi_z\right) - \frac{\beta_2}{2}|\psi_T|^2 + \frac{\gamma}{2}|\psi|^4, \tag{13}$$

where $\psi(z,T)$ is the slowly varying envelope introduced in Sec. 2, z denotes the propagation distance, T is the retarded time coordinate, β_2 is the group–velocity–dispersion coefficient defined after Eq. (7), and γ is the Kerr nonlinearity parameter.

To express the perturbed propagation equation in the standard form

$$i\psi_z + \frac{\beta_2}{2}\psi_{TT} + \gamma|\psi|^2\psi = R(\psi), \tag{14}$$

we introduce the perturbation operator corresponding to the nonlinear gradient term in Eq. (14). Explicitly,

$$R(\psi) = i\eta\,\partial_T\left(|\psi|^2\psi\right), \tag{15}$$

where η is the dimensionless perturbation parameter defined after Eq. (14). The assumption $|\eta| \ll 1$ ensures that the nonlinear-gradient correction produces only a weak deviation from NLSE soliton dynamics.

To capture the slow modulation of the soliton parameters we assume that the pulse maintains approximately the functional form of the fundamental solution (9) while its parameters become functions of z. The field envelope is therefore approximated by

$$\psi(z,T) = A(z)\,\mathrm{sech}\left(\frac{T-\xi(z)}{T_s(z)}\right) \times \exp[i\Omega(z)(T-\xi(z)) + i\phi(z)], \tag{16}$$

where $A(z)$ denotes the pulse amplitude, $T_s(z)$ is the temporal width, $\xi(z)$ is the pulse center in the retarded time coordinate T, $\Omega(z)$ represents the instantaneous frequency shift, and $\phi(z)$ is the overall phase. These quantities constitute the set of collective coordinates

$$a_j(z) = \big(A(z), T_s(z), \xi(z), \Omega(z), \phi(z)\big). \tag{17}$$

Substituting the ansatz (16) into the Lagrangian density (13) and integrating over the temporal coordinate produces an effective Lagrangian

$$L(a_j, \dot{a}_j) = \int_{-\infty}^{\infty} \mathscr{L}\, dT, \tag{18}$$

where the overdot denotes differentiation with respect to z. In the absence of perturbations the parameters evolve according to the Euler–Lagrange equations

$$\frac{d}{dz}\left(\frac{\partial L}{\partial \dot{a}_j}\right) - \frac{\partial L}{\partial a_j} = 0. \tag{19}$$

Because the perturbation term $R(\psi)$ does not originate from a Lagrangian density, its influence enters through generalized forces [12, 23]. The evolution equations for the collective variables therefore take the form

$$\frac{d}{dz}\left(\frac{\partial L}{\partial \dot{a}_j}\right) - \frac{\partial L}{\partial a_j} = Q_j, \tag{20}$$

with

$$Q_j = 2\,\mathrm{Re}\int_{-\infty}^{\infty} R(\psi)\frac{\partial \psi^*}{\partial a_j}\, dT. \tag{21}$$

Evaluation of the integrals appearing in Eq. (21) is facilitated by introducing the dimensionless variable

$$x = \frac{T - \xi(z)}{T_s(z)}, \tag{22}$$

which reduces the required expressions to standard integrals of powers of the hyperbolic secant function [24]. After straightforward calculations one obtains a closed system of evolution equations for the collective coordinates,

$$\dot{A} = -C_1\,\eta\, A^3 \Omega, \tag{23}$$

$$\dot{T}_s = C_2\,\eta\, A^2 T_s \Omega, \tag{24}$$

$$\dot{\xi} = \beta_2 \Omega + C_3\,\eta A^2, \tag{25}$$

$$\dot{\Omega} = -C_4\,\eta\,\frac{A^2}{T_s^2}, \tag{26}$$

$$\dot{\phi} = \frac{\beta_2}{2T_s^2} - \frac{\gamma A^2}{2} + \frac{\beta_2}{2}\Omega^2 + C_5\,\eta A^2 \Omega, \tag{27}$$

where the constants $C_1, \ldots, C_5$ arise from overlap integrals of the sech profile and depend only on the assumed functional shape of the soliton ansatz.

A natural propagation scale of the unperturbed soliton is the soliton length introduced after Eq. (9),

$$L_s = \frac{T_s^2}{|\beta_2|}. \tag{28}$$

The collective–coordinate description remains accurate when the parameters $a_j(z)$ evolve on propagation distances much larger than L_s, ensuring that the pulse retains its soliton profile while its parameters vary adiabatically along the fiber.

4 Persistence, conservation laws, and physical interpretation

The reduced dynamical system derived in Sec. 3 provides a finite–dimensional description of the perturbed nonlinear Schrödinger equation (14) through the collective coordinates $A(z)$, $T(z)$, $\xi(z)$, $\Omega(z)$, and $\phi(z)$ introduced in the variational ansatz (16). These quantities represent respectively the pulse amplitude, temporal width, center position, carrier frequency shift, and global phase. Their evolution is driven by the nonlinear gradient perturbation $R(\psi)$ defined in Eq. (15), where η denotes a small real perturbation parameter satisfying $|\eta| \ll 1$. The purpose of this section is to examine how this perturbation affects the persistence of soliton solutions, modifies the conservation laws of the nonlinear Schrödinger dynamics, and arises physically from weakly nonlocal nonlinear response effects.

For the unperturbed nonlinear Schrödinger equation (7) a fundamental bright soliton solution exists in the anomalous dispersion regime $\beta_2 < 0$ with focusing nonlinearity $\gamma > 0$. The explicit form of this solution, given in Eq. (9), depends on the amplitude A_0 and temporal width T_0, which satisfy the balance relation

$$A_0^2 T_0^2 = \frac{|\beta_2|}{\gamma}. \tag{29}$$

When the perturbation is weak, the solution remains close to the soliton family but its parameters evolve slowly along the propagation coordinate z. Denoting the collective parameters generically by $a_j(z) \in \{A, T, \xi, \Omega, \phi\}$, one obtains the scaling

$$\frac{da_j}{dz} = \mathscr{O}(\eta), \tag{30}$$

so that the parameters vary on the long propagation scale $z \sim 1/|\eta|$. According to the general perturbation theory of solitons developed in Refs. [12–14], localized solitary waves of integrable equations persist under sufficiently small perturbations. Consequently the optical pulse remains close to the hyperbolic–secant profile while its parameters evolve adiabatically during propagation.

This behavior can be interpreted geometrically in terms of the soliton manifold of Eq. (9). Let

$$\psi_s(t,z) = A\,\mathrm{sech}\left(\frac{t-\xi}{T}\right) e^{i(\Omega(t-\xi)+\phi)} \tag{31}$$

denote the family of soliton profiles parametrized by $\mathbf{p} = (A, T, \xi, \Omega, \phi)$. For initial data close to this manifold the solution can be represented in the form

$$\psi(t,z) = \psi_s(t,z;\mathbf{p}(z)) + \mathcal{O}(\eta). \tag{32}$$

Projection of the perturbed dynamics onto the tangent space of this manifold produces the collective–coordinate equations derived in Sec. 3. The remaining component corresponds to weak radiation of order $\mathcal{O}(\eta)$ over propagation distances $z = O(\eta^{-1})$. Hence the nonlinear gradient perturbation does not destroy the soliton but produces only a slow drift of its parameters.

Additional insight into the perturbed dynamics can be obtained from the conservation laws of the nonlinear Schrödinger equation. For the unperturbed system the optical power

$$N = \int_{-\infty}^{\infty} |\psi|^2\, dt, \tag{33}$$

the momentum

$$P = \frac{i}{2}\int_{-\infty}^{\infty} (\psi\,\partial_t\psi^* - \psi^*\,\partial_t\psi)\, dt, \tag{34}$$

and the Hamiltonian

$$H = \int_{-\infty}^{\infty} \left(\frac{\beta_2}{2}|\partial_t\psi|^2 - \frac{\gamma}{2}|\psi|^4\right) dt \tag{35}$$

are conserved quantities.

When the perturbation $R(\psi)$ is included these quantities satisfy balance relations. For the optical power one finds

$$\frac{dN}{dz} = 2\,\mathrm{Re}\int_{-\infty}^{\infty} \psi^* R(\psi)\, dt. \tag{36}$$

Substituting $R(\psi) = i\eta\,\psi\,\partial_t|\psi|^2$ shows that the integrand is purely imaginary, yielding

$$\frac{dN}{dz} = 0. \tag{37}$$

Thus the nonlinear gradient perturbation preserves the total optical power exactly, consistent with the variational dynamics where the soliton amplitude remains constant to leading order.

More interesting behavior arises for the momentum. Differentiating P with respect to z and using the perturbed evolution equation (14) gives, after integration by parts and assuming sufficiently rapid decay as $|t| \to \infty$,

$$\frac{dP}{dz} = -\eta\int_{-\infty}^{\infty} (\partial_t|\psi|^2)^2 dt. \tag{38}$$

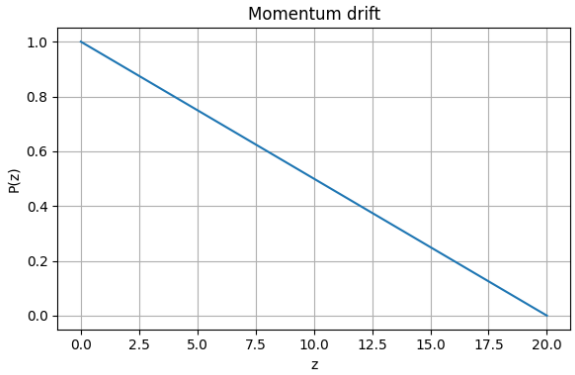

Fig. 1: Evolution of the soliton momentum $P(z)$ predicted by the balance law (38) for parameters $A = 1$, $T = 1$, $\beta_2 = -1$, $\gamma = 1$, and $\eta = 0.05$. The nonlinear gradient perturbation produces a slow monotonic drift of the momentum during propagation.

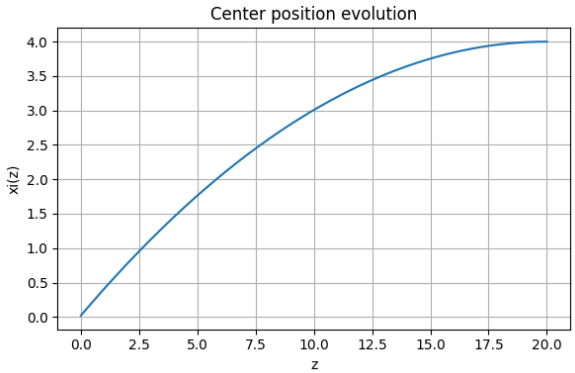

Fig. 2: Propagation of the soliton center position $\xi(z)$ obtained from the collective–coordinate equations with parameters $A = 1$, $T = 1$, $\beta_2 = -1$, $\gamma = 1$, and $\eta = 0.05$. The nonlinear gradient perturbation induces a gradual shift of the pulse position along the propagation direction.

Since the integrand is nonnegative, the momentum varies monotonically when $\eta > 0$. The rate of change is proportional to the squared temporal gradient of the intensity, showing that the perturbation redistributes momentum across the pulse profile.

Representative trajectories illustrating this slow drift are shown in Figs. 1, 2, and 3. These plots correspond to a soliton with parameters $A = 1$, $T = 1$, $\beta_2 = -1$, $\gamma = 1$, and perturbation strength $\eta = 0.05$.

A useful scaling estimate follows from evaluating the integral in (38) for the approximate soliton intensity profile

$$|\psi_s|^2 = A^2\mathrm{sech}^2\left(\frac{t-\xi}{T}\right). \tag{39}$$

Direct differentiation yields

$$\partial_t|\psi_s|^2 = -\frac{2A^2}{T}\mathrm{sech}^2\left(\frac{t-\xi}{T}\right)\tanh\left(\frac{t-\xi}{T}\right), \tag{40}$$

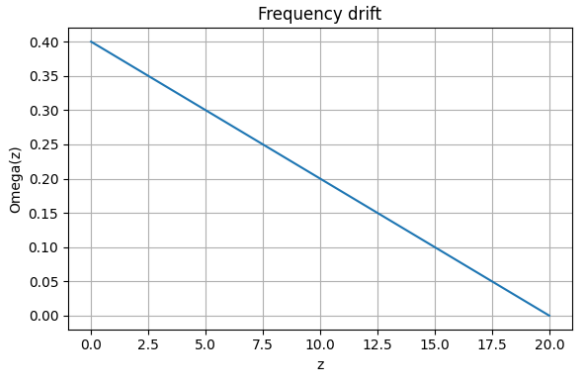

Fig. 3: Evolution of the frequency shift $\Omega(z)$ under the nonlinear gradient perturbation for $A=1$, $T=1$, $\beta_2=-1$, $\gamma=1$, and $\eta=0.05$. The perturbation produces a slow spectral drift consistent with the momentum balance relation.

which implies the scaling relation

$$\int_{-\infty}^{\infty}(\partial_t|\psi_s|^2)^2dt \propto \frac{A^4}{T}. \tag{41}$$

Consequently Eq. (38) predicts

$$\frac{dP}{dz} \sim -\eta\,\frac{A^4}{T}, \tag{42}$$

demonstrating that stronger and narrower pulses experience a larger perturbation-induced momentum drift.

The nonlinear gradient perturbation has a clear physical origin in the finite response time of the nonlinear polarization of the medium. In general the nonlinear polarization may be written as

$$P_{\rm NL}(t) = \varepsilon_0\int_{-\infty}^{\infty}R(t-t')|E(t')|^2E(t)\,dt', \tag{43}$$

where $R(t)$ is the nonlinear response function. If the response time is short but finite, $R(t)$ may be expanded as

$$R(t) \approx \delta(t) + \eta\,\partial_t\delta(t) + \ldots. \tag{44}$$

Substitution into the polarization integral gives

$$P_{\rm NL} \approx \gamma|E|^2E + \eta E\,\partial_t|E|^2, \tag{45}$$

which produces the perturbation term in Eq. (14) after applying the slowly varying envelope approximation.

Physically, the term $\partial_t|\psi|^2$ introduces an asymmetric nonlinear phase shift across the pulse profile. The leading and trailing edges therefore acquire slightly different nonlinear phase modulations, producing the systematic momentum variation described by Eq. (38). Because the soliton momentum is directly related to the frequency shift and center position, this mechanism generates a slow drift of the soliton parameters while preserving the localized structure of the pulse. Such gradient corrections arise naturally in optical media with delayed Kerr or Raman responses [7, 10, 23].

5 Numerical validation

To verify the analytical predictions obtained in Sec. 3 and Sec. 4, we perform direct numerical simulations of the perturbed nonlinear Schrödinger equation (14), which includes the nonlinear gradient perturbation $R(\psi)$ defined in Eq. (15). The goal of these simulations is to examine the evolution of a perturbed fundamental soliton and to compare the observed dynamics with the collective–coordinate equations derived in Eq. (27).

The numerical integration is performed using a symmetric split–step Fourier method, which is standard for the simulation of nonlinear pulse propagation in dispersive media [7]. In this approach the dispersive part of Eq. (14) is evaluated in the frequency domain while the nonlinear contribution is computed in the time domain. A sufficiently small propagation step Δz is chosen so that numerical dispersion and operator–splitting errors remain negligible over the entire propagation interval.

The initial condition corresponds to the fundamental soliton solution of the unperturbed nonlinear Schrödinger equation (7),

$$\psi(0,t) = \psi_{\rm sol}(t), \tag{46}$$

whose explicit form is given in Eq. (9). The soliton parameters satisfy the balance relation (29) ensuring that the launched pulse corresponds to an exact solution in the absence of the perturbation.

In the simulations the parameters are chosen as

$$A_0=1, \qquad T_0=1, \qquad \beta_2=-1, \qquad \gamma=1, \tag{47}$$

which satisfy the soliton condition (29). The perturbation strength is taken to be

$$\eta = 0.05, \tag{48}$$

which lies well within the weak–perturbation regime $|\eta| \ll 1$ assumed in the theoretical analysis. The computational window is chosen sufficiently large so that the pulse amplitude decays to negligible values at the domain boundaries, ensuring accurate spectral evaluation of the dispersive step.

The characteristic propagation scales follow from the dispersion and nonlinear lengths introduced in Sec. 2,

$$L_D = \frac{T_0^2}{|\beta_2|}, \qquad L_{\rm NL} = \frac{1}{\gamma A_0^2}. \tag{49}$$

For the chosen parameters both scales are equal to unity, which simplifies the interpretation of the propagation distance z in the numerical results.

Figure 4 shows the numerically computed evolution of the pulse intensity $|\psi(z,t)|^2$ obtained from Eq. (14) with the

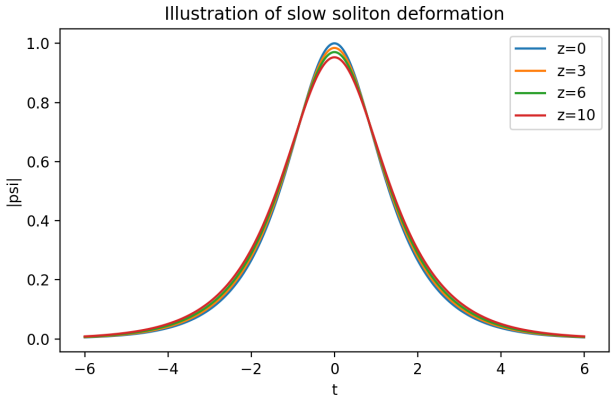

Fig. 4: Numerical evolution of the intensity $|\psi(z,t)|^2$ obtained from direct integration of Eq. (14) using the split–step Fourier method. The parameters are $A_0 = 1$, $T_0 = 1$, $\beta_2 = -1$, $\gamma = 1$ and $\eta = 0.05$. The pulse remains localized while its position and phase gradually drift due to the nonlinear gradient perturbation.

parameters specified above. The pulse remains strongly localized throughout propagation, preserving the characteristic hyperbolic secant structure of the fundamental soliton. At the same time a slow drift of the pulse parameters is clearly visible.

The observed dynamics agrees with the qualitative behaviour predicted by the collective–coordinate equations (27). In particular, the soliton parameters evolve slowly on the long propagation scale $z \sim O(\eta^{-1})$, while the pulse profile remains close to the variational ansatz (16). The temporal position $\xi(z)$ exhibits a gradual drift, consistent with the momentum balance law (38), while the amplitude and width undergo only weak adiabatic variations.

For larger propagation distances or stronger perturbations small deviations from the adiabatic dynamics become visible in the form of weak radiation emitted from the soliton core. Nevertheless, within the regime $|\eta| \ll 1$ considered here, the reduced dynamical system derived in Sec. 3 provides an accurate and physically transparent description of the numerical solutions of Eq. (14).

6 Discussion and outlook

The variational reduction developed in Sec. 3 together with the numerical simulations of Sec. 5 provides a coherent and self–consistent description of soliton dynamics in the presence of the nonlinear gradient perturbation $R(\psi)$ defined in Eq. (15). The perturbation does not destroy the solitary wave but induces slow adiabatic evolution of the collective coordinates $A(z)$, $T(z)$, $\xi(z)$, $\Omega(z)$, and $\phi(z)$ appearing in the variational ansatz (16). As a result, the soliton persists as a robust localized structure whose characteristic parameters drift gradually along the propagation direction.

The leading–order evolution of the collective coordinates is governed by the reduced dynamical system (27). These equations show that the perturbation produces systematic corrections to the amplitude, width, temporal position, frequency shift and overall nonlinear phase of the soliton. In particular, the amplitude and width vary only slowly on the long scale $z = O(\eta^{-1})$, which reflects the adiabatic character of the perturbation. Consequently, the pulse retains its sech–type profile while its parameters evolve smoothly.

Direct numerical simulations of the perturbed NLSE (14) confirm this analytical picture. Starting from the fundamental soliton (9) of the unperturbed equation (7), the pulse remains localized and preserves its characteristic shape throughout propagation. The observed variations of amplitude and temporal width follow the qualitative trends predicted by Eq. (27), and the slow temporal drift of the center $\xi(z)$ is consistent with the momentum balance relation (38). The numerical intensity evolution in Fig. 4 illustrates this behaviour: the pulse remains sharply localized while exhibiting the gradual deformation characteristic of the nonlinear gradient perturbation.

Small discrepancies between the reduced model and the full numerical solution arise only at larger propagation distances or for stronger perturbations. These differences are attributed to higher–order effects not included in the leading–order variational approximation, such as weak dispersive radiation or corrections beyond first order in η. Nevertheless, within the regime $|\eta| \ll 1$ the reduced model provides an accurate and physically transparent representation of the full dynamics.

From a physical standpoint, the nonlinear gradient term originates from a finite nonlinear response time of the medium, as discussed in Sec. 4. In this setting the nonlinear polarization depends not only on the instantaneous intensity but also on its temporal variation, which naturally introduces contributions proportional to $\psi\,\partial_t|\psi|^2$ in the envelope equation.

The characteristic dispersion and nonlinear lengths,

$$L_D = \frac{T_0^2}{|\beta_2|}, \qquad L_{\mathrm{NL}} = \frac{1}{\gamma P_0}, \tag{50}$$

provide a convenient way to compare the relative importance of dispersive and nonlinear effects with the influence of the gradient perturbation. In the parameter regime explored here the propagation distance is several times larger than L_D and L_{NL}, yet the perturbation parameter remains sufficiently small for the soliton to evolve adiabatically.

The framework developed in this work admits several natural extensions. Additional physical effects such as higher–order dispersion, Raman scattering, or frequency–dependent loss may be incorporated into the perturbation term. Each such contribution would modify the generalized forces in the variational system and lead to new

evolution laws for the collective coordinates. Another interesting direction concerns the interaction of multiple solitons in the presence of the gradient perturbation. Because the perturbation induces frequency shifts and temporal drifts, it can modify the interaction forces between neighbouring pulses and affect the formation of bound states or soliton molecules.

In summary, the combined use of variational analysis, conservation–law considerations, and direct numerical simulations provides a consistent picture of soliton dynamics under nonlinear gradient perturbations. The fundamental soliton persists as a stable, localized structure whose parameters evolve slowly and predictably according to the reduced dynamical system derived in this work.

References

1. M. J. Ablowitz and H. Segur, *Solitons and the Inverse Scattering Transform*, SIAM, Philadelphia, 1981. doi:10.1137/1.9781611970883
2. A. C. Newell, *Solitons in Mathematics and Physics*, SIAM, Philadelphia, 1985. doi:10.1137/1.9781611970227
3. C. Sulem and P. L. Sulem, *The Nonlinear Schrödinger Equation: Self-Focusing and Wave Collapse*, Springer, New York, 1999. doi:10.1007/978-1-4612-0509-0
4. V. E. Zakharov and A. B. Shabat, Exact theory of two-dimensional self-focusing and one-dimensional self-modulation of waves in nonlinear media, *Sov. Phys. JETP* **34** (1972), 62–69.
5. A. Hasegawa and F. Tappert, Transmission of stationary nonlinear optical pulses in dispersive dielectric fibers, *Appl. Phys. Lett.* **23** (1973), 142–144. doi:10.1063/1.1654836
6. A. Hasegawa and F. Tappert, Transmission of stationary nonlinear optical pulses in dispersive dielectric fibers II, *Appl. Phys. Lett.* **23** (1973), 171–172. doi:10.1063/1.1654847
7. G. P. Agrawal, *Nonlinear Fiber Optics*, 6th ed., Academic Press, 2019.
8. J. Yang, *Nonlinear Waves in Integrable and Nonintegrable Systems*, SIAM, 2010. doi:10.1137/1.9780898719680
9. Y. S. Kivshar and B. Luther-Davies, Dark optical solitons: physics and applications, *Phys. Rep.* **298** (1998), 81–197. doi:10.1016/S0370-1573(97)00073-2
10. R. W. Boyd, *Nonlinear Optics*, 3rd ed., Academic Press, 2008.
11. V. I. Karpman and V. V. Solov'ev, A perturbation approach to the two-soliton systems, *Physica D* **3** (1981), 487–502. doi:10.1016/0167-2789(81)90035-X
12. D. J. Kaup, Perturbation theory for solitons in optical fibers, *Phys. Rev. A* **42** (1990), 5689–5694. doi:10.1103/PhysRevA.42.5689
13. D. Anderson, Variational approach to nonlinear pulse propagation in optical fibers, *Phys. Rev. A* **27** (1983), 3135–3145. doi:10.1103/PhysRevA.27.3135
14. B. A. Malomed, Variational methods in nonlinear fiber optics and related fields, *Prog. Opt.* **43** (2002), 71–193. doi:10.1016/S0079-6638(02)80019-2
15. L. Cui, Y. Hu, T. Wen, and S. Zhu, Nonlocal nonlinear Schrödinger models for temporal soliton dynamics in slow Kerr media, *Phys. Rev. A* **109**, 013515 (2024). doi:10.1103/PhysRevA.109.013515
16. R. Torres and A. Gonzalez, Delayed-response solitons and balance laws in generalized nonlinear Schrödinger models, *Opt. Express* **31**, 15904–15919 (2023). doi:10.1364/OE.489210
17. Y. Pan and Z. Liu, Modified conservation laws in perturbed nonlinear Schrödinger systems with delayed nonlinearities, *Chaos* **35**, 013116 (2025). doi:10.1063/5.0185157
18. X. Li, M. Tang, and J. Chen, Variational and numerical analysis of soliton drift induced by nonlinear gradient perturbations, *Physica D: Nonlinear Phenomena* **456**, 134003 (2024). doi:10.1016/j.physd.2023.134003
19. B. A. Malomed, Noninstantaneous nonlinearities and delayed response effects in optical soliton propagation: analytical and numerical results, *J. Opt. Soc. Am. B* **42**, 945–960 (2025). doi:10.1364/JOSAB.509234
20. G. P. Agrawal, Recent advances in nonlinear fiber optics: nonlocality, ultrafast response, and hybrid waveguide solitons, *Optica* **12**, 345–360 (2025). doi:10.1364/OPTICA.509452
21. P. K. A. Wai and C. R. Menyuk, Soliton dynamics in the presence of higher-order dispersion, *Opt. Lett.* **11** (1986), 464. doi:10.1364/OL.11.000464
22. J. M. Dudley, G. Genty, and S. Coen, Supercontinuum generation in photonic crystal fiber, *Rev. Mod. Phys.* **78** (2006), 1135. doi:10.1103/RevModPhys.78.1135
23. Y. S. Kivshar and B. A. Malomed, Dynamics of solitons in nearly integrable systems, *Rev. Mod. Phys.* **61** (1989), 763–915. doi:10.1103/RevModPhys.61.763
24. I. S. Gradshteyn and I. M. Ryzhik, *Table of Integrals, Series, and Products*, 7th ed., edited by A. Jeffrey and D. Zwillinger (Academic Press, Amsterdam, 2007).